Hindawi
Geofluids
Volume 2018, Article ID 4934520, 19 pages
https://doi.org/10.1155/2018/4934520

Research Article

Geochemical Fingerprinting of Rising Deep Endogenous Gases in an Active Hypogenic Karst System

A. Fernandez-Cortes,[1] **R. Perez-Lopez**,[2] **S. Cuezva**,[1] **J. M. Calaforra**,[1] **J. C. Cañaveras**,[3] **and S. Sanchez-Moral**[4]

[1]*Department of Biology and Geology, University of Almeria, 04120 Almeria, Spain*
[2]*Geological Hazard Division, Geological Survey of Spain (IGME), 28003 Madrid, Spain*
[3]*Department of Environment and Earth Sciences, University of Alicante, 03690 Alicante, Spain*
[4]*Department of Geology, National Museum of Natural Sciences (MNCN-CSIC), 28006 Madrid, Spain*

Correspondence should be addressed to A. Fernandez-Cortes; acortes@ual.es

Received 4 May 2018; Revised 15 September 2018; Accepted 25 September 2018; Published 6 December 2018

Academic Editor: Marco Petitta

Copyright © 2018 A. Fernandez-Cortes et al. This is an open access article distributed under the Creative Commons Attribution License, which permits unrestricted use, distribution, and reproduction in any medium, provided the original work is properly cited.

The hydrothermal caves linked to active faulting can potentially harbour subterranean atmospheres with a distinctive gaseous composition with deep endogenous gases, such as carbon dioxide (CO_2) and methane (CH_4). In this study, we provide insight into the sourcing, mixing, and biogeochemical processes involved in the dynamic of deep endogenous gas formation in an exceptionally dynamic hypogenic karst system (Vapour Cave, southern Spain) associated with active faulting. The cave environment is characterized by a prevailing combination of rising warm air with large CO_2 outgassing (>1%) and highly diluted CH_4 with an endogenous origin. The $\delta^{13}C_{CO2}$ data, which ranges from −4.5 to −7.5‰, point to a mantle-rooted CO_2 that is likely generated by the thermal decarbonation of underlying marine carbonates, combined with degassing from CO_2-rich groundwater. A pooled analysis of $\delta^{13}C_{CO2}$ data from exterior, cave, and soil indicates that the upwelling of geogenic CO_2 has a clear influence on soil air, which further suggests a potential for the release of CO_2 along fractured carbonates. CH_4 molar fractions and their δD and $\delta^{13}C$ values (ranging from −77 to −48‰ and from −52 to −30‰, respectively) suggest that the methane reaching Vapour Cave is the remnant of a larger source of CH_4, which was likely generated by microbial reduction of carbonates. This CH_4 has been affected by a postgenetic microbial oxidation, such that the gas samples have changed in both molecular and isotopic composition after formation and during migration through the cave environment. Yet, in the deepest cave locations (i.e., 30 m below the surface), measured concentration values of deep endogenous CH_4 are higher than in atmospheric with lighter $\delta^{13}C$ values with respect to those found in the local atmosphere, which indicates that Vapour Cave may occasionally act as a net source of CH_4 to the open atmosphere.

1. Introduction

Hypogene karstification is generally related to the rising of CO_2- or H_2S-rich fluids, and aggressiveness of the waters is obtained by cooling the fluids in the oxidation zone, not only in the water bodies but also in the air by condensation-corrosion processes. Caves form by the specific conditions of hypogene speleogenesis and that their active hydrogeochemical mechanisms (e.g., hydrothermal input, sulphuric acid, mixing corrosion, dissolution of evaporites, and dissolution in mixed sulphate-carbonate sequences [1–3]) can potentially harbour subterranean atmospheres with distinctive gas compositions. One example of this is when abiotic CO_2 and CH_4 gases are formed by chemical reactions that do not directly involve organic matter. This composition results from current activity or residual signs of degassing from gas-enriched groundwater or geothermal focus at depth. Consequently, this represents a mixture of multiple sources.

The migration of deep endogenous gases plays a key role in the formation of macroscopic void-conduit systems under hypogenic settings. Hypogenic karst regions are widely

distributed throughout the world [3]. However, there have been few studies addressing the gas composition of the subterranean atmospheres currently undergoing hypogene speleogenesis, and the few that exist have primarily focused on sulphidic caves (e.g., [4]). Air monitoring in the Frasassi Caves of Italy revealed a remarkable outgassing of both CO_2 and H_2S from the groundwater, which varied seasonally from 1 to 8 ppm for H_2S and from 1500 to 5600 ppm for CO_2. In this system, the rapid gas exchange with the upper, non-sulphidic levels maintains a normal oxygen concentration [5]. Ascending warm water with H_2S and CO_2 degassing, high salinity from dissolved chlorides, sulphides, high noble gas concentrations, and radioactive decay have been described as the main factors existing in hyperkarst phenomena along active deep-rooted faults [6]. Recently, it has been noted that the oxidation of CH_4 influences the generation of sulphides during sulphuric acid speleogenesis in active systems [7]. This presents a new and valuable dataset of CH_4 concentrations and stable-isotope ratios of hydrogen and carbon in CH_4 found within the air of actively forming sulphidic caves.

Most hypogenic caves formed by the movement of thermal waters in phreatic settings are now located far above the water table and are thus no longer active. One exception to this pattern may be represented by caves associated with active faulting and geothermal areas where there are high concentrations and releases of upwelling fluids of endogenous origin, which enhance the processes and distinctive features of hypogene karstification [8–12]. As an example, venting of subcrustal CO_2 has been described in a hydrothermal cave associated with an active, deep-rooted fault [13]. Recent works deal with the importance of seismic characterization of these systems since faults act as preferential migration routes of the ascending fluids that contribute to the formation of the hypogenic karstic system [14].

Vapour Cave (VC) in southern Spain represents a hypogenic system related to upwelling of deep endogenous fluids from an active faulting zone. The pathways and mechanisms that control the exchange of deep endogenous gases among atmosphere, soil, and subsurface reservoirs in VC have not been characterized to date. This study is aimed at characterizing the specific constraints imposed by an active hypogenic system such as that found in VC in the dynamics of deep-sourced gases (carbon dioxide and methane) with potential for release into the open atmosphere. Here, we provide insights into the behaviour of these deep endogenous gases in the upper vadose zone of karst terrains in active faulting zones. Isotope ratios of carbon and hydrogen imprinted in the rising geogenic gases (CO_2 and CH_4) in this hypogenic cave are used to investigate the sourcing and biogeochemical processes involved in the release, storage, and consumption of these gases into the upper vadose zone, and their interaction with the lower troposphere.

2. Geological Context and Hydrogeological Settings

VC is located within the Murcia Province of SE Spain (Figure 1), along the southern side of a small carbonates butte in the village of Alhama de Murcia. This small butte is part of the *Sierra Espuña*, and it is directly related to the Alhama de Murcia Fault (AMF), a tectonically active, NE-SW-trending master fault with a left lateral strike-slip and a reverse component. The last earthquake attributed to this fault was in May of 2011, during which nine people were killed, and many rock-falls and ground cracks affected a total area of nearly 1000 km^3 around the epicentre zone [15]. Cave development affected Miocene (Lower Tortonian) conglomerates with rounded pebbles of carbonate and metamorphic rocks [16]. This unit is related to a postorogenic mantle of carbonate units structured by reverse faults, which have since changed to strike-slip tectonics. Convergence between Africa and the microplate of Iberia has uplifted the mountains of *Sierra de Carrascoy* and *Sierra Espuña* along a dominantly NE-SW trend.

The study zone of Alhama de Murcia is located within the Segura River basin (SE of Spain) (Figure 1). The hill where VC is located (namely, "Cerro del Castillo," at 319 m a.s.l) has been traditionally related with the quaternary alluvial deposits of the Low Guadalentin aquifer. However, the last studies [17] established a hydrological connection with the western carbonates belonging to the Santa Yechar aquifer (namely, Santa Yechar-Alhama aquifer), which are quite massive, of Triassic age, and with an average thickness of 150 m. Therefore, the hydric recharge primarily happens in southern foothills of Sierra Espuña mountains, where the main carbonate outcrops of the Santa Yechar aquifer are located (Figure 1). The superficial area of the Santa Yechar-Alhama aquifer is 58 km^2.

Figure 2 summarizes the main geological units where this aquifer is embedded in the vicinity of VC. The main permeable unit of this aquifer is formed by 150 m thickness of Triassic black dolostones (Tr in Figure 2), from the Alpujárride Complex. On this unit and showing discordance appears 100 m of polygenic conglomerates of Tortonian age (G in Figure 2, host-rock of Vapour Cave) and a stratum of red sandstone and conglomerates of middle-lower Tortonian age (A in Figure 2). The impermeable units at the bottom correspond to Permo-Triassic phyllites (Pz in Figure 2), of the Intermediate Betic Units and Alpujárride Complex. At local scale, the aquifer is laterally sealed by marls of middle-lower Tortonian age, which form the relief of the northern mountains (Sierra de la Muela), and to the south with the late Miocene marls with gypsum located below the quaternary alluvial deposits (m and R in Figure 2, respectively).

At regional scale, the structure of this aquifer is determined by three mega nappes caused by an overthrust with south dip. This tectonic structure determines that the groundwater bodies of this aquifer are linked to the location of each one of these nappes, which are widely compartmentalised by an extensive faulting system. The most superficial one has been overexploited. In the deepest water body, the piezometric levels are below the sea level (with depths in boreholes ranging 350–400 m), whereas the piezometric level in the intermediate one ranges 96–188 m a.s.l. [17]. The hydrochemical facies of the two deeper water bodies are of sulphate-calcium type. The small

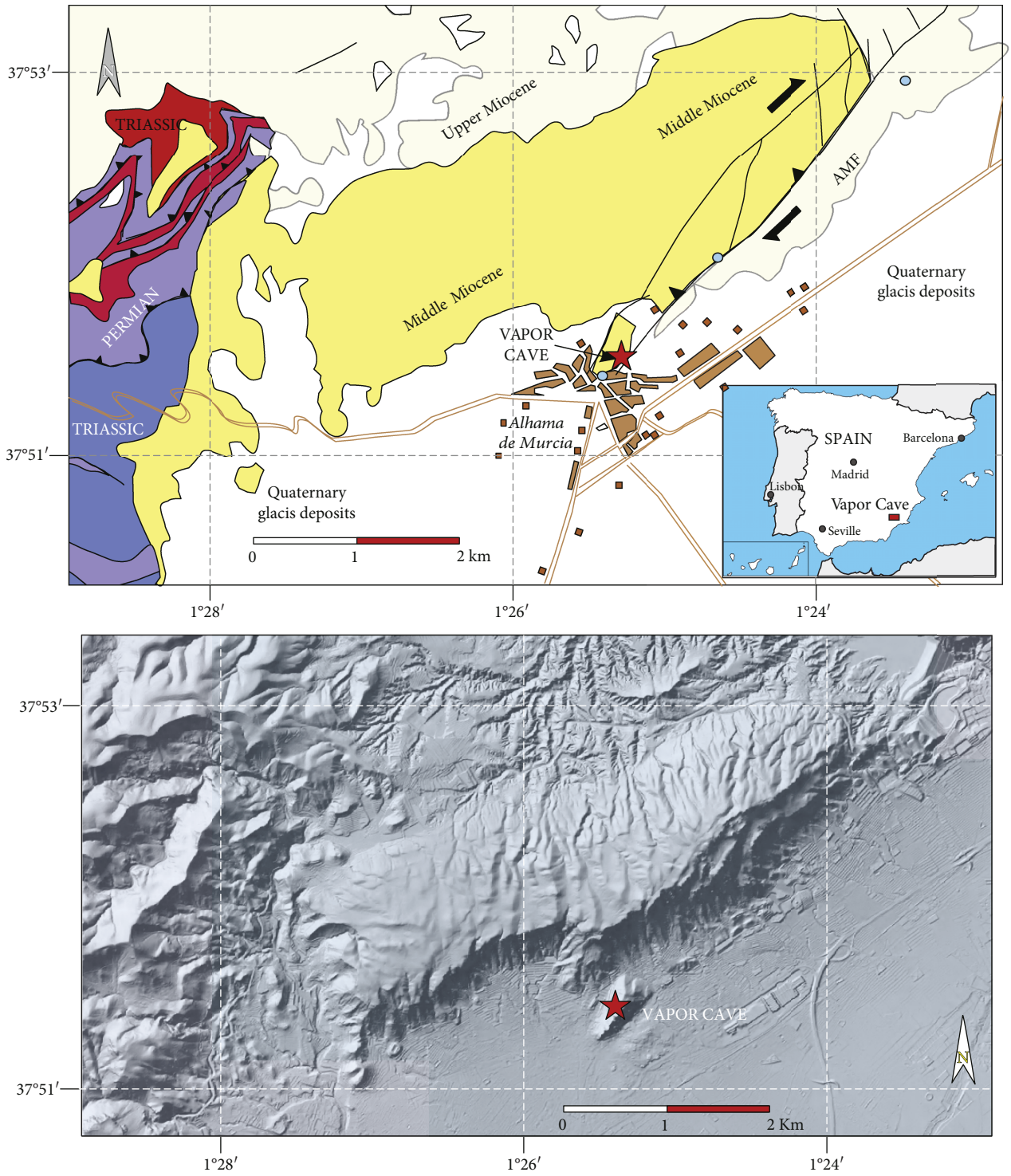

Figure 1: Location, local geological settings, and digital terrain model of the study area in relation to the Alhama de Murcia Fault (AMF).

upland where VC is located belongs to the intermediate buckled strata, as well as the thermal boreholes displayed in Figures 2 and 3.

Besides the Alhama de Murcia Fault (NE-SW-trending, Figure 2), the local geometry of the aquifer determines that the VC site is in the middle of consecutive reverse faults with opposite dips. This faulting system results in an alternation in depth of the black Triassic dolostones (Tr) or Tortonian conglomerates with the younger red sandstones and conglomerates of the middle-lower Tortonian age (A) cross-section of Figure 2 and lithological column of borehole 1 and 2 in Figure 3.

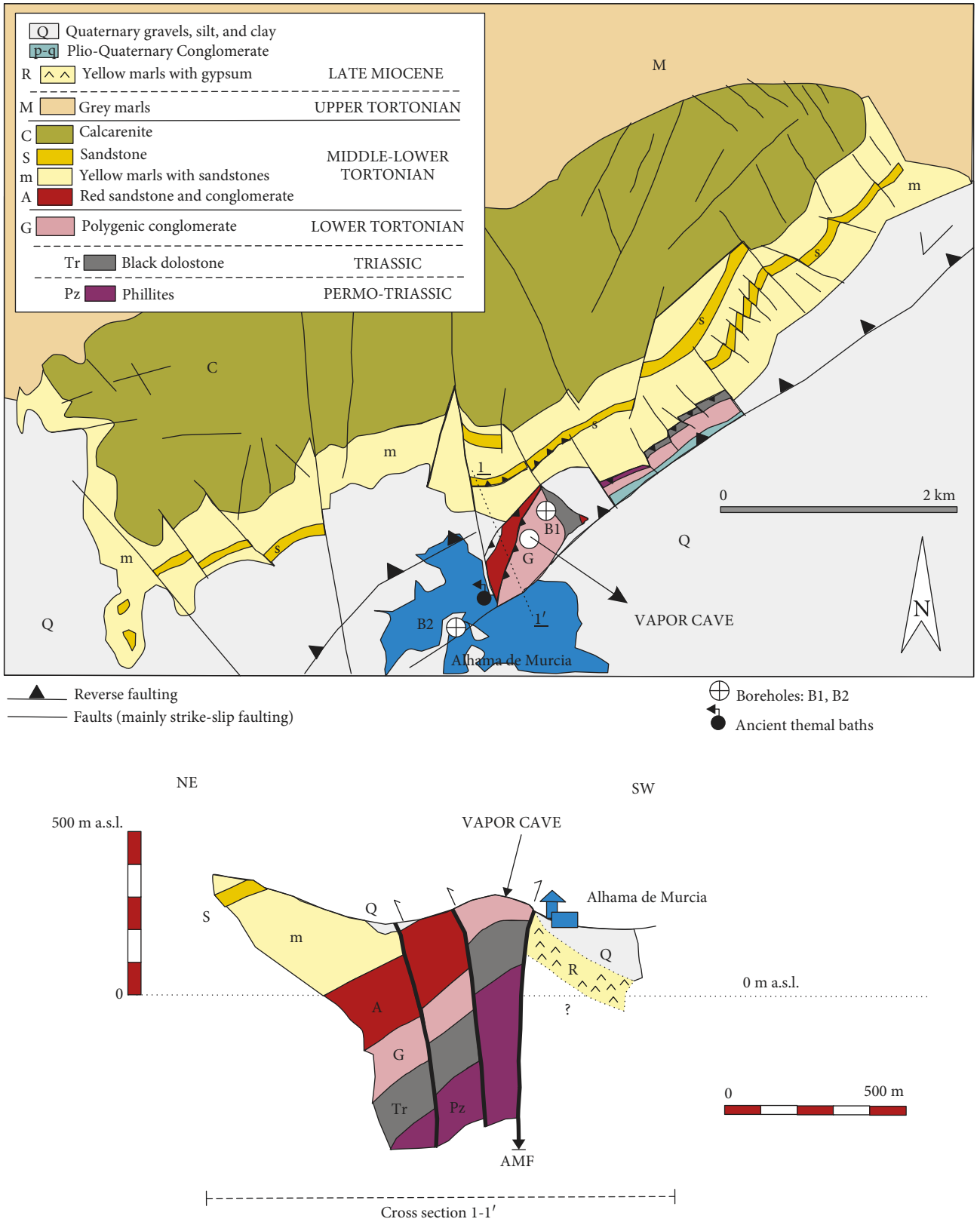

Figure 2: Geological map of the study area with main geological units (strata and faults) that set up the local hydrological features in the vicinity of Vapour Cave. Locations of the cave and two key boreholes are indicated and further discussed in Figure 3.

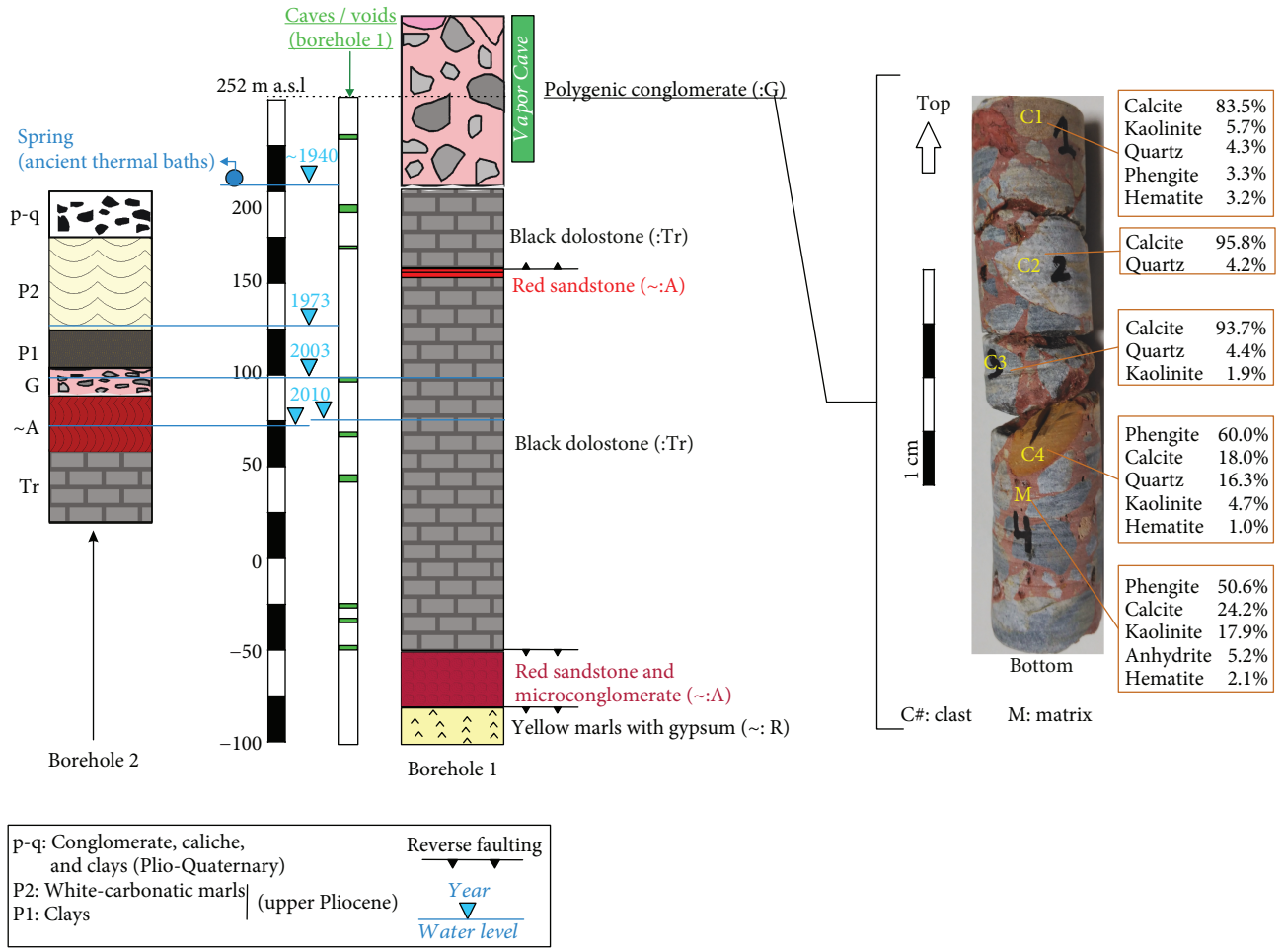

FIGURE 3: Lithological columns of two key boreholes near Vapour Cave; "Cerro del Castillo" (borehole 1) and "Agua de Dios" (borehole 2), both of them linked to the ancient thermal baths of Alhama de Murcia (southern Spain) (adapted from [17] and other unpublished technical reports provided by the Alhama de Murcia city council). Time evolution of water table and depths of the karstified sections (presence of caves and voids) are displayed in relation to lithologic units. The mineral composition (DRX analysis) of both clasts and matrix of a small core sample of the polygenic conglomerate (host rock of Vapour cave) is also detailed.

The Alhama de Murcia Fault would control the flux of groundwater by two ways (Figure 2, low panel with the geological cross section):

(1) The relative subsidence of the SW block of materials (Quaternary deposits and late Miocene marls with gypsum) provokes the contact of the Triassic dolostones with the impermeable marls, and consequently, the circulation of groundwater towards southeast is hindered.

(2) The elevation of the northwest block of materials (including the conglomerates hosting Vapour Cave and the lower aquifer of Triassic dolostones) enhanced the circulation of deep and thermal groundwater towards the surface. The local discharge of thermal groundwater was historically located in the layer contact between the dolostones and the overlying conglomerates, just on the natural spring of thermal water that fed the ancient baths at Alhama de Murcia. Nowadays, the piezometric surface is located at variable depths depending on the extractions destined to irrigation in the whole aquifer.

Figure 3 shows the lithological columns of two key boreholes near VC. Borehole 1 (namely, "Cerro del Castillo") is 350 m deep, and it is located 197 m far from the entrance to Vapour cave at 252 m a.s.l. Borehole 2 (namely, "Agua de Dios") is located in the downtown of Alhama de Murcia, and it was drilled up to 180 m depth aimed at supplying hot water to the local thermal baths. This second borehole is at 202 m a.s.l and approximately 780 m far from VC.

Geothermal activity has been reported in both boreholes, with water temperature of 41.4°C at borehole 1 and ranging 39.8–41.0°C at borehole 2 [17, 18], values in concordance with the historical records of temperature for the spring water that fed the ancient thermal baths [19].

Borehole 1 is quite representative of lithology below VC, particularly providing information about the strata just below de Tortonian conglomerates that host the cave. Figure 3 also includes the mineralogical composition of the polygenic conglomerate of Tortonian age. The mineralogical

composition was analysed by powder X-ray diffraction in a Philips PW 1710/00 diffractometer (National Museum of Natural Sciences, Madrid) using CuKα radiation with a Ni filter and a setting of 40 kV and 40 mA. Data were collected and interpreted using the XPowder software package. The qualitative search-matching procedure was based on the ICDD-PDF2 database. There is a high percentage of calcite clasts, which were cemented with a phengite matrix. Thick packets of phengite have been described for the Triassic materials of the Alpujárride Complex in southern Sierra Espuña [20], near the study site but at higher elevations. Phengite of the polygenic conglomerates likely came from weathering of these emerged Triassic materials and then transported with clasts through alluvial systems to the coastline, where conglomerates were formed during the lower Tortonian.

Vapour cave (VC), at 295 m a.s.l, only breaks through the Conglomerates of Tortonian age, but its deepest conduits (roughly at −80 m depth) do not reach the black Triassic dolostones, at least through human-size paths. These dolostones should appear in just 13 meters, approximately, below the bottom of the cave and locally house the water table of the aquifer.

During the drilling works of borehole 1, it was also registered in the lithological column the data of depths with caves and voids due to karstification (Figure 3). Borehole 1 crosses through a 4 m high cave in the polygenic conglomerates, which would be located at 65 m depth in the vertical section of Vapour Cave. The remainder of the caves crossed by borehole 1 is embedded into the layer of Triassic black dolostones, with heights ranging 1 to 5 meters [17]. This karstified section of the dolostone strata proves the existence of other trapped air pockets, particularly below Vapour Cave, with a likely presence of endogenous gases that can be potentially released to the exterior atmosphere throughout the faulting system or smaller fissures. Vapour Cave would be a single case of subterranean air pocket that has made its way outwards through the overlying conglomerates.

The records on borehole 2 confirm a continuous decrease in the piezometric level due to overexploitation of the whole aquifer Santa Yechar-Alhama, from the extinct natural spring (roughly at 200 m a.s.l) to water below 75 m a.s.l. in the last decade (Figure 3). Therefore, the vadose (unsaturated) conditions of the local aquifer have gone prevailing progressively during the last decades and, consequently, the percentage of air reservoirs in the karstified dolostones has increased in the same way. By considering a current hydrostatic level in the local aquifer in a range of 50–75 m a.s.l (located in the dolostone strata in both boreholes), the estimated thickness of unsaturated rock (polygenic conglomerates plus black dolostones) below VC would reach 140–165 m.

3. Cave Settings

VC represents a chasm in a karstic area of active faulting and developed in a favourably fissured carbonate-cemented conglomerate host rock under hypogene speleogenesis by the upwelling of hydrothermal (38–43°C, and 100% relative humidity) and CO_2-rich fluids, in or from the zone of fluid-geodynamic influence. In addition to high air temperatures, VC presents other extreme values of some environmental parameters, such as hypoxic conditions (17% O_2), CO_2 concentrations that exceed 1%, radon (^{222}Rn) activity with values above 50 kBq/m^3, and a vertical thermal gradient of 3.2°C/100 m. All of these conditions have been associated with the combined effects of tectonic activity and hydrothermalism [16]. The current thermal gradient is capable of sustaining free convection of rising $H_20_{(V)}$ and CO_2 outgassed from endogenous CO_2-rich waters. Consequently, active carbonic acid dissolution still occurs as a hypogenic agent.

The deepest explored part of VC is associated with ancient Roman baths (*Baños de Alhama*), which were exploited during many cultural periods in the village (Roman, Muslim, Medieval, and Modern ages). Geochemical analyses of groundwater at this location have been performed [21]. Groundwater temperature was found to have a mean value of 41°C; a pH of 6.8 was documented, and the concentrations of Cl^- and HCO_3^- suggested the presence of carbonated water. The isotopic signal of dissolved carbon dioxide ranges $-8‰ < \delta^{13}C_{CO2} < -4‰$, in agreement with the thermal degradation of carbonates.

VC is a hypogenic cave that developed in two well-defined sections, subvertical gallery and vertical shafts, with a total explored depth of 84 m below the surface (Figure 2). The first gallery is a subhorizontal tube with an oval section and 50 m of developed marginal outlets, which contain small voids. It appears to be a master passage sloping downward to 30 m below the surface, which developed in carbonate fissures and near-surface fissures running perpendicular to AMF (Figure 2). It constitutes a laterally extensive network with some small "blind-ended" passages, some of which serve as conduits for lateral migration of fluids to the nearest outlet feature (e.g., "ventilador gallery"). The uppermost part of this gallery exhibits the typical morphogenetic features of an outlet conduit, with some cupolas and vertical channels that rise from the ceiling, one of which connects with the exterior through a single, narrow entrance located at the highest point. The cave entrance is oval-shaped, and the axes measure 0.6×0.75 m. This master passage is connected to a vertical feeding channel (50 m long) that reaches 84 m deep and is related to the AMF fault plane (NE-SW-trending). The chasm becomes narrower as it reaches the lower vadose zone, and it constitutes the main conduit of rising flow of endogenous gases. The bottom of the feeder channel is obscured by the presence of sediment in-fill and breakdown blocks of conglomerate fallen from upper levels; some swallowing or entrenchment forms can also be distinguished.

4. Cave Monitoring, Air Sampling Procedures, and Gas Analytical Techniques

A cave air monitoring, gas sampling, and analytical protocol was developed to obtain the key data for understanding the cave-soil-atmosphere system, including temperature, and gaseous composition of the air (molar fractions of CO_2 and CH_4 and $\delta^{13}C_{CO2}$, δ^2H_{CH4}, and $\delta^{13}C_{CH4}$ values). Monitoring

was conducted via in situ spot measurements, and air samples were analysed in a laboratory setting.

In situ and discrete air sampling as well as spot measurements were conducted during intensive surveys lasting for several hours each. The deepest locations were only accessible by very experienced speleologists with self-contained breathing apparatuses due to low oxygen content, extreme temperatures, and hazardous concentrations of other gases. Consequently, *in situ* measurements and air sampling at these deeper locations were only conducted when feasible, and always with the technical assistance of the Mountain Rescue Team (GERA) of the Firefighter's Service of Madrid Autonomous Region.

Overall, eight air-sampling campaigns were conducted from 2015 to 2017 during September of 2015, March and November of 2016, and April and June–September of 2017. The air-sampling campaigns span two hydrogeological cycles, i.e., from September 2015 to August 2016 and from September 2016 to August/September 2017. The two most recent sampling campaigns (August and September of 2017) also included analyses of δ^2H_{CH4} in air samples, which were performed within 2 weeks of sample acquisition. Spot sampling of cave air was typically conducted in a predefined network of points that were spatially distributed at several depths: 2, 15, 30, 50, and 80 m below the surface, as well as in randomly distributed locations throughout the cave (Figure 2). The background atmosphere at the exterior was sampled along a transect from the cave entrance until reaching 32 meters far from it. Cave air and exterior atmosphere samples were collected at 1 m above the floor using a portable air compressor (Aquanic s790) running at 0.4 L·min^{-1}. Samples for soil gas analyses were collected at several fixed sites located vertically above the cave, and using a 6 mm OD steel tube with grooved sides at each end, and inserted to a depth of 30–50 cm through undisturbed soils to the bedrock-soil interface. Soil air was extracted using a microdiaphragm gas pump (KNF Neuberger, Freiburg, Germany) at 3.1 L·min^{-1} at atmospheric pressure. All air samples were collected into 1 L Tedlar bags with a lock valve design specifically to ensure inertness and gas tightness. Air samples from the soil were collected during the same time slot as the sampling of cave air and background atmosphere at the exterior, then all of them were analysed in the laboratory for determining the gas composition (molar fractions of CO_2 and CH_4, and for $\delta^{13}C_{CO2}$ and $\delta^{13}C_{CH4}$ values) within 48 hours following the sample collection on field.

Spot measurements of air temperature, relative humidity, air pressure, and CO_2 concentrations were also taken in the same cave locations as the cave air samples and from the cave exterior using handheld devices (XP100 and XP200, Lufft) with integrated air pressure sensors (measurement range: 800–1100 mbar, accuracy at 25°C and 1013.25 mbar, max. ±0.5 mbar), an external temperature probe (PT100 1/10 DINB probe, with an accuracy of ±[0.03+ 0.002*measurement]), and a capacity probe for relative humidity (measurement range: 0–100%, accuracy: ±3% above 90%). All devices had certified calibrations. Furthermore, a multigas monitor (MX6 iBrid, Industrial Scientific) was used for quantification of CO_2 and O_2 concentrations of cave air, including safety warning levels, and those of other gases potentially present in hypogene environments (e.g., H_2S, VOCs, and H_2). Further technical details may be found at http://www.indsci.com/products/multi-gas-detectors/mx6/.

During the last two field campaigns, the installation of a multichannel system to collect samples from the cave entrance, and at five depths within the cave, 2, 15, 30, 50, and 80 m below the surface, was completed. This system consists of a 100 m long hose with 5 flexible PVC tubes of 25, 50, 75, and 100 m lengths, respectively, such that the end of each tube is located at the aforementioned depths. Cave air was extracted using a microdiaphragm gas pump (KNF Neuberger, Freiburg, Germany) at 4.5 L·min^{-1} at 1.5 bar. To minimize the effects of water condensation in the tubes, a laboratory gas drying unit (i.e., a polycarbonate tube with filters, and filled with Drierite desiccant) was installed before filling the Tedlar bags. Finally, a multigas MX6 iBrid monitor was connected in sequence to the sampling tubes and enclosed in an air-tight box to measure the gas concentrations of the air collected at each depth.

Air samples were analysed at the National Museum of Natural Sciences (Spanish National Research Council-CSIC) for determining CO_2 and CH_4 molar fractions, as well as the isotopic $\delta^{13}C$ values for both gases using wavelength-scanned cavity ring-down spectroscopy (CRDS-WS). A Picarro G2201-i CRDS analyser (Picarro Inc., USA) was used to quantify the isotopologues of carbon dioxide and methane and to automatically calculate the carbon isotopic value for both gases with high precision. According to the manufacturer's technical specifications, this CRDS analyser measures the isotopologues of carbon dioxide ($^{12}CO_2$ and $^{13}CO_2$) with a precision of 200 ppb (±0.05 of reading) and 10 ppb (±0.05 of reading) for $^{12}CO_2$ and $^{13}CO_2$, respectively, resulting in a precision greater than 0.16‰ for $\delta^{13}C_{CO2}$ after 5 min of analysis. The measurements of methane isotopologues ($^{12}CH_4$ and $^{13}CH_4$) reached a precision of 5 ppb (±0.05 of reading) and 1 ppb (±0.05 of reading) for $^{12}CH_4$ and $^{13}CH_4$, respectively, resulting in a precision greater than 1.15‰ for $\delta^{13}C_{CH4}$ after 5 min of analysis.

Air samples in duplicate Tedlar bags were sent to the Institute for Marine and Atmospheric research (IMAU, Utrecht University) for high-precision measurements of hydrogen isotopes on atmospheric methane (and $\delta^{13}C_{CH4}$ for some samples) by using continuous-flow isotope ratio mass spectrometry (CF-IRMS) and following previously published methods [22]. This method separates CH_4 from other air components by utilizing purely physical processes based on temperature, time, and mechanical valve switching (i.e., without any added chemicals), and the purified sample is then pyrolysed to H_2 for stable isotope measurements. This analytical procedure allows high-precision measurements of δD and $\delta^{13}C$ from atmospheric CH_4 samples, with typical reproducibility of ±0.07‰ for $\delta^{13}C$, 2.3‰ for δD, and 17 ppb for CH_4 concentrations. For the CF-IRMS analyses, the amount of sample gas was adjusted to yield the same amount of CH_4 for each measurement. The general atmospheric measurement setup of the CF-IRMS analyser was adjusted by adding an ascarite/Mg $(ClO_4)_2$ filter to remove the preexisting large amounts of CO_2. To measure samples

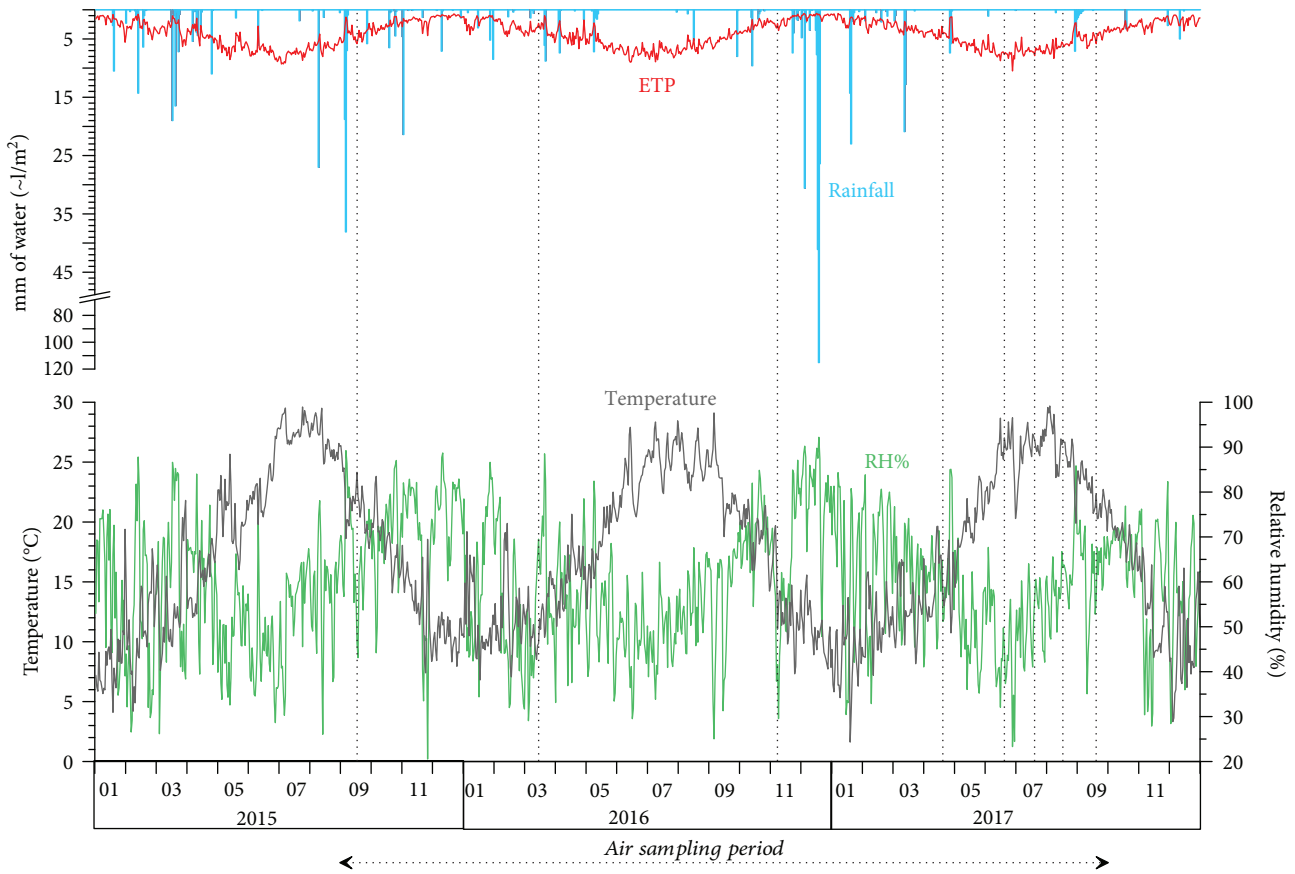

Figure 4: Daily meteorological conditions in the study area from January 2015 to December 2017, including the dates of the air sampling campaigns (dotted vertical lines). Parameters; air temperature, relative humidity, rainfall, and evapotranspiration according to the Penman-Monteith FAO parameterization scheme [25].

with lower CH_4 content, this method was further adjusted to extract CH_4 from larger volumes of air. The stable carbon and hydrogen isotope compositions of both gases (CO_2 and CH_4) are expressed as $\delta^{13}C$ and $\delta^{2}H$ relative to standards Vienna Pee Dee Belemnite (VPDB) and Vienna Standard Mean Ocean Water (VSMOW).

Three in-house standards with certified gas mixtures and known CO_2 and CH_4 concentrations (6993 ppm, 399 ppm, and zero-CO_2 and 0.5 ppm, 1.7 ppm, and zero-CH_4, respectively, supplied by Praxair Spain) were processed regularly at the beginning and at the end of each analytical session to verify the proper functioning of the CRDS analyser. Further details about the methodological procedures and quality results can be found elsewhere [23]. Additionally, we periodically evaluated $\delta^{13}C_{CH4}$ measurements by processing diluted air samples extracted from the following standard gases with certified methane stable isotope ratios: T-iso3 (250 ppm CH_4 and −38.3‰ $\delta^{13}C_{CH4}$) and L-iso1 (2500 ppm CH_4 and −66.5‰ $\delta^{13}C_{CH4}$), both supplied by Isometrics Instruments (Canada). In-house standards were also subjected to quality control by comparing the results obtained with the Picarro G2201-i analyser with duplicated bags collected from cylinders and subsequently analysed independently in the greenhouse gas laboratory at the Royal Holloway University of London (RHUL). There, gas concentrations were analysed with a Picarro G1301 CRDS analyser, and $\delta^{13}C_{CO2}$ and $\delta^{13}C_{CH4}$ were measured in triplicate by CF GC-IRMS using a GV Instruments Trace Gas e IsoPrime system [24]. Finally, duplicated air samples collected in situ were also analysed for $\delta^{13}C_{CH4}$ by CF-IRMS (IMAU, Utrecht) and then compared with measurements provided by the Picarro G2201 CRDS analyser, confirming an agreement between both analyses. Overall, these internal and intercomparison procedures periodically validated that the performance specifications regarding CO_2 and CH_4 analyses via a CRDS analyser were met.

5. Results

During the first hydrological cycle, the timing of access to the cave and air sampling was determined by availability of the qualified speleologists abovementioned. The sampling campaigns were intensified during the second hydrological cycle thanks to the installation of the multichannel system to collect samples from the cave entrance, i.e., without need to access the cave. In this period of two hydrological cycles, 8 field campaigns were conducted, 5 of which included sampling up to 30 m deep, and 3 of which included air sampling up to 80 m deep.

The daily meteorological conditions in the study area during the sampling period are shown in Figure 4, including the dates of the air sampling campaigns. Table 1 summarizes

Table 1: Climate conditions in the study are during the last two decades, including the annual-average values of main climatic parameters: air temperature, relative humidity, rainfall, and evapotranspiration according to the Penman-Monteith FAO parameterization scheme [25].

Hydrological year	T_avgr (°C)	RH_avgr (%)	Rainfall (mm) ETP	PM_FAO (mm)
Sept. '96–Aug. '97	17.08	68.7	271	1210
Sept. '97–Aug. '98	17.70	67.1	242	1239
Sept. '98–Aug. '99	17.35	64.1	206	1268
Sept. '99–Aug. '00	17.36	65.5	135	1250
Sept. '00–Aug. '01	17.95	63.3	183	1319
Sept. '01–Aug. '02	17.20	66.6	416	1192
Sept. '02–Aug. '03	18.09	62.7	212	1262
Sept. '03–Aug. '04	17.55	67.7	360	1161
Sept. '04–Aug. '05	17.22	67.2	132	1340
Sept. '05–Aug. '06	17.19	70.2	316	1308
Sept. '06–Aug. '07	17.70	69.2	344	1359
Sept. '07–Aug. '08	16.81	67.1	305	1376
Sept. '08–Aug. '09	16.54	59.8	319	1423
Sept. '09–Aug. '10	16.64	66.2	520	1330
Sept. '10–Aug. '11	16.59	64.1	189	1384
Sept. '11–Aug. '12	17.06	58.3	128	1575
Sept. '12–Aug. '13	16.52	59.9	355	1424
Sept. '13–Aug. '14	17.41	57.4	95	1560
Sept. '14–Aug. '15	17.60	58.6	266	1531
Sept. '15–Aug. '16	17.32	59.5	187	1491
Sept. '16–Aug. '17	17.51	60.8	382	1459
Average year	17.26	64.0	265	1355

the evolution of climate during the last two decades, including the annual-average values of main climatic parameters: air temperature, relative humidity, rainfall, and evapotranspiration. These climate data sets were supplied by a meteorological station at Alhama de Murcia, belonging to the Network of the Agricultural Information System of Murcia (http://siam.imida.es/) and located at 169 m a.s.l and less than 7 km far from Vapour Cave.

The area has a semiarid Mediterranean climate. The average annual temperature is 17.26°C, ranging 16.5–18.1°C over the last two decades. During the sampling period, the minimum values of the daily average temperature were recorded in the winter months of December/January, ranging 8.5–10.4°C, and the highs in the summer months of July/August (25.7–27.8°C). The average annual relative humidity (RH) is 64%, historically ranging from 57.4% to 70.2%. During the sampling period, the minimum values of the daily average RH were recorded from May to July, usually below 50%, and the highs in October (>60%).

Rainfall in the area is typical of a semiarid climate: 265 mm/year on average during the last two decades, with some cycles under very dry conditions (<100 mm/year). Annual rainfall for a whole hydrological cycle has ranged from 187 to 380 mm during the sampling period (2015–2017). The annual evapotranspiration is five times higher than precipitations (this difference factor ranged from 3.8 to 7.9 during the last two hydrological cycles), which results on prevailing xeric conditions.

It has a very marked dry season in the summer, a period in which more than 3 months (May to July/August) are usually registered without any precipitation or, at least, rainfall lower than 5 mm/month. During the rest of the year, precipitation events are very scarce and are distributed between winter, spring, and autumn, but without a constant pattern (e.g., very low rainfall is registered during some winter months). Low rainfall on an annual scale is opposed to the existence of some torrential events, for instance, 194 mm during just five days (15–19 December 2016).

The mean value of measured CO_2 and CH_4 concentrations and their stable isotopic compositions ($\delta^{13}C_{CO2}$ and $\delta^{13}C_{CH4}$) in the cave environment, above-cave soils, and local exterior atmosphere are shown in Table 2. Soil-CO_2 concentrations were relatively low, with heavy $\delta^{13}C_{CO2}$ values in all samples, and range from 527 ppm in September of 2015 to 2034 ppm in September of 2017 following moderate rainfall (3.5 L m^{-2}). Values of $\delta^{13}C$-CO_2 of soil air ranging from −9.8 to −15.9‰ are consistent with a local semiarid climate.

The local outdoor atmosphere has mean values of CO_2 and CH_4 concentrations slightly above the recent global monthly mean CO_2 (roughly 405 ppm and 1.85 ppm, respectively, check https://www.esrl.noaa.gov/gmd/ccgg/data-products.html for our monitoring period). The highest CO_2 values were recorded in the autumn, coinciding with colder outdoor air temperatures.

Table 2: Mean measurements (and ±sd: standard deviation) for the concentrations of CO_2 and CH_4, and their stable isotopic compositions ($\delta^{13}C_{CO2}$ and $\delta^{13}C_{CH4}$) in the cave environment, and in vertically adjacent soils and the local outdoor atmosphere.

	CO_2 (ppm)		$\delta\ ^{13}c_{c02}$ (%)		CH_4 (ppm)		$\delta\ ^{13}c_{cH4}$ (%)		n
	avgr	± sd	avgr	± sd	avgr	± sd	avgr	± sd	
Sep. '15									
Soil	527	6	−9.83	0.15	1.80	0.00	−46.89	0.80	4
Cave	8257	1795	−5.77	0.56	1.09	0.16	−42.57	3.31	8
Ext.	411	2.06	−8.26	0.16	1.91	0.01	−47.55	0.39	4
Mar. '16									
Soil	810	218	−11.80	0.53	1.86	0.12	−46.36	0.57	4
Cave	9040	2575	−6.29	0.83	2.62	0.49	−49.17	1.95	9
Ext.	—	—	—	—	2.06	0.02	−48.10	0.45	4
Nov. '16									
Soil	1907	929	−15.60	2.33	0.52	0.55	−44.07	5.30	5
Cave	11.964	1535	−5.83	0.32	0.87	0.06	−44.43	16.42	9
Ext.	503	153	−7.84	0.58	2.03	0.01	—	4.28	4
Apr. '17									
Soil	1472	1430	−15.87	0.56	0.71	0.61	−42.66	6.34	3
Cave	7507	2036	−6.35	0.43	1.08	0.14	−45.95	1.64	10
Ext.	465	20	−10.71	0.51	2.01	0.01	−51.93	0.64	3
Jun. '17									
Soil	1035	702	−12.46	1.60	1.76	0.37	−45.33	0.20	3
Cave	7775	979	−5.56	0.12	0.95	0.06	−35.29	2.22	5
Ext.	434	271	−9.25	1.29	2.16	0.08	—	5.49	4
Jul. '17									
Soil	639	87	−12.79	0.57	1.88	0.18	−47.20	1.72	3
Cave	8998	1718	−5.72	0.08	0.94	0.22	−41.40	16.31	3
Ext.	433	193	−8.08	1.10	2.04	0.04	—	0.83	3
Aug. '17									
Soil	649	329	−11.07	0.18	1.94	0.12	−47.68	3.39	4
Cave	10.441	1230	−5.35	0.16	0.89	0.12	−38.66	5.31	6
Ext.	434	16	−9.07	0.65	2.00	0.00	−53.08	0.46	3
Sep. '17									
Soil	2034	646	−13.45	1.89	0.50	0.06	−62.89	4.02	3
Cave	12.251	3251	−5.60	0.50	1.07	0.09	−39.41	7.09	8
Ext.	417	9	−8.65	0.09	1.99	0.00	—	1.23	3
Average									
Soil	**1134**	**543**	**−12.86**	**0.98**	**1.37**	**0.25**	**−47.88**	**2.79**	**29**
Cave	**9529**	**1890**	**−5.81**	**0.38**	**1.19**	**0.17**	**−42.11**	**6.78**	**58**
Ext.	**442**	**95**	**−8.84**	**0.63**	**2.02**	**0.02**	**−50.17**	**1.72**	**28**

All of the underground samples presented higher concentrations of CO_2 and higher $\delta^{13}C_{CO2}$ than those of the exterior atmosphere and soil air. The underground air exhibits high concentrations of CO_2 that generally increase with depth. This general trend is broken at 15 m depth by the existence of an external air intake through the "Ventilador" gallery (Figure 5) that causes a decrease in the concentration of CO_2 and a concomitant increase in the concentration of CH_4. The effect of this air intake intensifies during cold periods (e.g., November of 2016), and it significantly influences the thermal and O_2 profiles. The mean annual concentration of CH_4 in the underground air is lower than that of both the soil and the outdoor atmosphere. Only in March of 2016 were CH_4 concentrations above the atmospheric background (ranging 2.3–3.4 ppm) detected. The $\delta^{13}C_{CO2}$ values of underground air ranged from −4.5 to −7.5‰, and the CH_4 molar fractions and both δD and $\delta^{13}C$ values ranged from −77 to 48‰ and −52 to −30‰, respectively.

The temperature profile of the cave interior reveals three clear divisions (Figure 5): (1) a shallow thermal zone from 0 to 15 m depth controlled by exterior air influx, (2) a

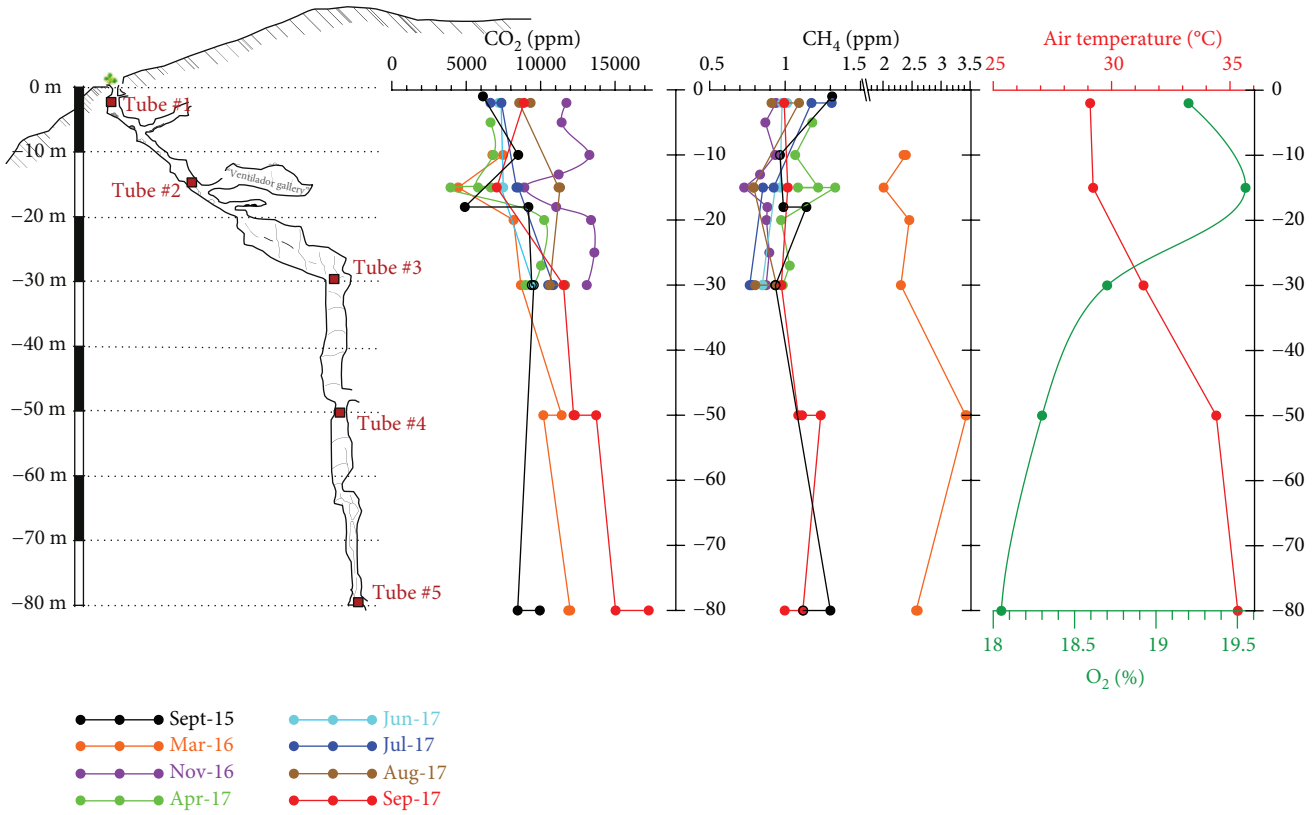

FIGURE 5: Spatiotemporal evolution of temperature and gaseous composition of cave air (CO_2, CH_4, and O_2 contents) along a vertical profile.

heterothermal medium zone between 15 and 50 m with a marked increase in temperature by 5°C at 35 m depth, and (3) the thermal deep zone with a progressive increase in temperature controlled by the geothermal gradient.

6. Discussion

6.1. Geochemical Tracing of CO_2 Sources and Dynamic at VC. The active hypogene speleogenesis at VC is mainly controlled by the upwelling airflow from the zone of fluid-geodynamic influence associated with an active fault with frequent microseisms [26]. Cave air samples have a remarkably high concentration of CO_2 with heavy $\delta^{13}C_{CO2}$ values (−5.81‰ on average, and ranging from −7.40 to −4.67‰), which indicates a clear deep endogenous source of CO_2 in cave air. These $\delta^{13}C_{CO2}$ values in air are also in agreement with those measured in CO_2-rich thermal waters of the aquifer spatially associated with the active fault (between −8.1 and −3.8‰ [21]). Therefore, degassing from CO_2-rich groundwater and deep-sourcing geothermal CO_2 seem to be the prevailing processes responsible for the high abundance of CO_2, and its heavier carbon isotopic composition. According to the historical piezometric records from some near boreholes, the local water level matches the layer of Triassic black dolostones below VC (roughly 140–165 m), which are highly karstified due to the chemical aggressiveness of this CO_2-rich groundwater. The network of karstic voids/caves and fissures below VC would favour the diffusion and convection of deep-endogenous gases to the upper layers of the aquifer, including the polygenic conglomerates hosting VC.

Similar carbon isotopic ratios have been described for soil air samples from hydrothermal areas within wider volcanic regions [27] and magma-derived CO_2 emissions [28]. Other studies at hydrothermal sites have described wider ranges of carbon isotope composition of CO_2 (e.g., from −2.4 to −7.8‰ in submarine hydrothermal vents [29] and from −1.0 to −9.1‰ in hot springs [30]). Taking these $\delta^{13}C_{CO2}$ values as references, a higher $\delta^{13}CO_2$ may indicate the addition of CO_2 directly from volcanic sources [31] or from underlying sedimentary rocks containing more marine carbonate minerals (i.e., CO_2 produced mainly by thermal decarbonation [32]). On the contrary, lighter $\delta^{13}CO_2$ values suggest a likely contamination by crustal organic sediments [33].

A Keeling analysis and modelling of the stable isotope fractionation of CO_2 and CH_4 was used to identify and assess the processes as consumption, accumulation, and mobilization (e.g., bacterial oxidation of CH_4 or diffusion of soil-derived or deep-sourced CO_2), as mixture of gases with distinguishable origins, or resulting from different consumption or production processes. In the case of CO_2 analysis for VC (Figure 6), the Keeling diagram incorporates the assumption that each data point corresponds to the gas composition of cave air, including molar fraction and isotopic value. It represents a mixture of two end-member gases: local atmosphere and pure CO_2 that have been added to the cave air to produce the composition at the observation point. The

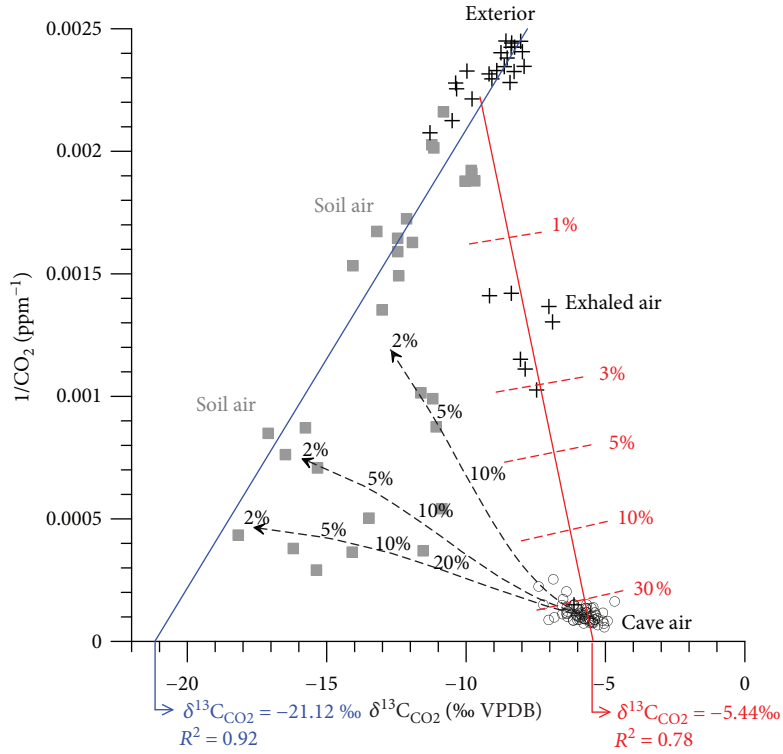

FIGURE 6: Plot of $1/CO_2$ versus $\delta^{13}C_{CO2}$ for soil (grey squares) and cave air (open circles). The composition of the local atmosphere is indicated by crosshairs, distinguishing those samples of exhaled air collected just inside the cave entrance. The Keeling functions fit the set of data points representing a two-component mixture of average atmospheric air with an additional source of CO_2, either the pure component from the soil (blue straight line, without considering the dispersed data point towards cave air), or from deep endogenous air (red straight line). Extrapolation down to the X-axis yields the $\delta^{13}C_{CO2}$ of the CO_2 source: soil-derived CO_2 (−21.12‰, $R^2 = 0.92$) and deep endogenous CO_2 (−5.44‰, $R^2 = 0.78$).

Keeling plot reveals the isotopic composition of this pure CO_2 by extrapolating the straight line joining the atmospheric end-member to the data point under consideration, as far as its intersection with the $\delta^{13}C_{CO2}$ axis [34]. This $\delta^{13}C_{CO2}$ value is only an apparent composition and does not correspond to a real source of CO_2 if there are other processes occurring (e.g., diffusion or mixing with several pure CO_2 sources that have more than a single composition for $\delta^{13}C_{CO2}$).

Thus, two sources of CO_2 are considered in this analysis through Keeling diagrams, either from soil or from deep endogenous air. The red keeling function in Figure 6 shows the effects of mixing between the atmosphere, and the composition of pure deep endogenous CO_2, considering a composition close to the maximum CO_2 concentration and $\delta^{13}C_{CO2}$ values measured for the cave air samples (17,623 ppm and −4.67‰, respectively) and the average composition of the local atmosphere (442 ppm and −9.01‰). Red dashed lines are contours of equal mixing ratios labelled as % of pure CO_2 remaining in the cave air samples, including the exhaled air from the cave entrance. According to this model, the underground air at VC usually maintains more than 30% pure theoretical CO_2 (with a $\delta^{13}C_{CO2} = -5.44$‰) added from a deep endogenous source. The mixing process with the local atmosphere increases as the upwelling flux of air travels to the cave entrance; thus, the exhaled air to the outdoor atmosphere represents between 1 and 3% of this pure theoretical CO_2 added from a deep endogenous source.

The blue Keeling function in Figure 6 shows the effects of mixing between the atmosphere and the composition of theoretical pure soil CO_2. The soil-derived CO_2 includes all CO_2 originally generated within the soil (i.e., from root respiration and soil organic matter degradation) as well as some subsequent processes (e.g., direct gas diffusion mainly from deeper soil layers or previously accumulated in the fissures, fractures, and pore spaces of rocks in the vadose zone). The extrapolation down to the X-axis gives $\delta^{13}C_{CO2}$ of the soil-derived CO_2 source of −21.12‰ ($R^2 = 0.92$). This value is consistent with CO_2 derived from the decomposition of C3 biomass (−27 ± 3‰) plus a 4.4‰ diffusional enrichment [35], but clearly distinguishable from the epigenetic caves characterized by a lighter end-member for soil CO_2 production with $\delta^{13}C_{CO2} = -26$‰ or less [36].

This $\delta^{13}C_{CO2}$ value also indicates that CO_2 produced by microbial respiration in soils containing organic material from C3 vegetation might not be the only process responsible for the concentration and carbon isotopic composition of soil CO_2. In fact, there are many data points for soil air that scatter closely under the best-fit line (blue Keeling plot in Figure 4), and therefore, these points seem to represent mixtures between atmospheric air and more than one single pure CO_2 end-member (i.e., they are not only from soil-derived CO_2).

Because the scatter of soil points is high, we have established a complementary model to explain the outliers of soil gas composition. This is based on how upwelling flow of deep

endogenous gases in this cave influences the $\delta^{13}C_{CO2}$ values of the soil air, which is likely due to an intense CO_2 diffusion from the cave to the soil layers located immediately above. This effect is noticeable because the data points from the soil air with the highest CO_2 concentrations tend to drift away in a perpendicular direction from the mixing line exterior-soil (blue keeling function in Figure 3) towards the data set of cave air with higher CO_2 content and heavier $\delta^{13}C_{CO2}$.

The curved dashed arrows in Figure 6 show the kinetic fractionation trajectory of deep endogenous CO_2 due to its upwards diffusion from cave air to soil layers through fissures and small-size cracks of deep soil-epikarst. Gas diffusion, driven by concentration gradients according to Fick's law, may produce ^{13}C depletion in the diffusing gas collected in the soil air samples, and consequently, the residual CO_2 gas in cave air will be ^{13}C-enriched. In any case, the diffusing gas that reaches the soil environment is ^{13}C-enriched with respect to the soil-derived CO_2 (i.e., from root respiration and soil organic matter degradation), which is identified with the data pairs better aligned to the mixing line exterior soil (blue Keeling plot in Figure 6). Gas diffusion is modelled by means of a Rayleigh-type distillation process with several kinetic fractionation coefficients (3.05‰, 2.60‰, and 1.77‰) in the function of the CO_2 gradient between cave air and the deepest layers of soil. The Rayleigh equation is an exponential relation that describes the partitioning of isotopes between two reservoirs as one reservoir decreases in size, in this case the CO_2 content in soil air. These kinetic fractionation coefficients result from fitting the Rayleigh-type distillation curves considering the average values of CO_2 concentration and $\delta^{13}C_{CO2}$ of cave air (9529 ppm and −5.81‰, respectively) and three representative soil CO_2 values ([2000 ppm, 18.48‰], [1175 ppm, 16.62‰], and [600 ppm, 13.18‰]), in accordance to the mixing line between soil air and local atmosphere (blue keeling function in Figure 6). There is an intense vapour condensation on cave wall and ceilings during the upwards flux of warm and humid air, which hinders the gaseous connection between the cave environment and the above soil layer through fissures, small size cracks, and the connected porous system. As a consequence, the kinetic fractionation coefficients used to model the CO_2 diffusion are lower than the theoretical mass-dependent fractionation between $^{12}CO_2$ and $^{13}CO_2$ during diffusion within the external soil layers (4.4‰ [37]). Each diffusion curve has been labelled as percentage of deep endogenous CO_2 that remains in the soil air after the gas diffusion process occurring between cave and soil. Some soil samples showed a remaining deep endogenous CO_2 that ranges between 5% and 10%, which demonstrates that the upwelling flow of geogenic CO_2 has a clear influence on the external soil above the cave.

6.2. Sources and Sink Processes during Migration and Upwelling of Deep Endogenous Methane. The $\delta^{13}C_{CH4}$ and $\delta^{2}H_{CH4}$ variations in cave air provide considerable insight into the nature of gas exchange and consumption processes controlling the CH_4 dynamic in underground environments. A key reference point in the data interpretation is that the background atmosphere usually has around 1.8 ppm of CH_4 and its carbon and hydrogen isotopic composition ($\delta^{13}C_{CH4} \approx -47$‰ VPDB, $\delta^{2}H_{CH4} \approx -100$‰ VSMOW) is a product of inputs from an isotopically wide range of sources. The CH_4 concentration of cave air in epigenetic caves and, in general, in well-ventilated caves independently of their speleogenesis mechanisms are often depleted, confirming that subterranean environments may represent an overlooked sink for atmospheric CH_4 [23, 38–44] and, further, it is rapidly consumed in caves on time scales ranging from hours to days [23, 39]. On the opposite case, underground air of some hypogene caves may contain unusually high levels of methane (up to 3%, e.g., Movile Cave) related to the action of chemoautotrophic bacteria [45], and others have moderate CH_4 concentrations, just above the atmospheric background, related to CH_4 outgassing from spring water in sulphuric acid hypogenic caves (e.g., <4 ppm CH_4 at Cueva Villa Luz [7]).

The variations of $\delta^{13}C_{CH4}$ as a function of methane concentrations in air of VC are illustrated in Figure 7, compared to a standard composition of the local atmosphere (CH_4: 2.02 ppm and $\delta^{13}C_{CH4}$: 50.17‰). The most relevant fact is that some noticeable concentrations of deep endogenous methane have been occasionally registered. Thus, in the deeper sites of this chasm (below 30 m and, particularly, at 50 m depth), deep endogenous CH_4 reaches values higher than the atmospheric background (ranging 2.3 to 3.4 ppm) with $\delta^{13}C_{CH4}$ values, a bit lighter with respect to those found in the local atmosphere (Figure 7). These data were registered for the first time during March of 2016, but no more evidences of high CH_4 concentration have been observed in the subsequent surveys on field for air sampling. These high concentrations of deep endogenous CH_4 denote a more intense migration of endogenous fluids through the upper vadose zone, which could be related with an increase in regional seismotectonic activity.

The general trend of the scattered data points in Figure 7 is that smaller CH_4 concentrations of cave air are associated with the most ^{13}C-enriched CH_4. These data suggest that methanotrophic oxidizing bacteria (MOB) seem to be the main responsible for consumption CH_4 in cave air. Curves of Figure 7 fit the locus compositions formed by MOB consumption of atmospheric CH_4, modelled as a Rayleigh process using several kinetic fractionation factors (F) and considering as starting point the maximum CH_4 concentration registered at 50 m depth in March of 2016, as a clear example of a deep endogenous source of this gas. This model for CH_4 consumption by MOB seems to work, since cave air samples with $\delta^{13}C_{CH4}$ values heavier than −50‰ are located within the plotted area defined by these distillation curves, and, likewise, data pairs with heavier $\delta^{13}C_{CH4}$ match with distillation curves with higher fractionation factors.

As a reference, the magnitude of kinetic fractionation factors associated with methane oxidation varies between 1.009 in anoxic aqueous environments [46] and 1.025–1.049 during gas transport in soils above landfill. The fractionation factors for samples of VC are within the range calculated for the aerobic oxidation of CH_4 from laboratory cultures of methanotrophs ([47, 48] and references therein) and field studies on the vadose zone above

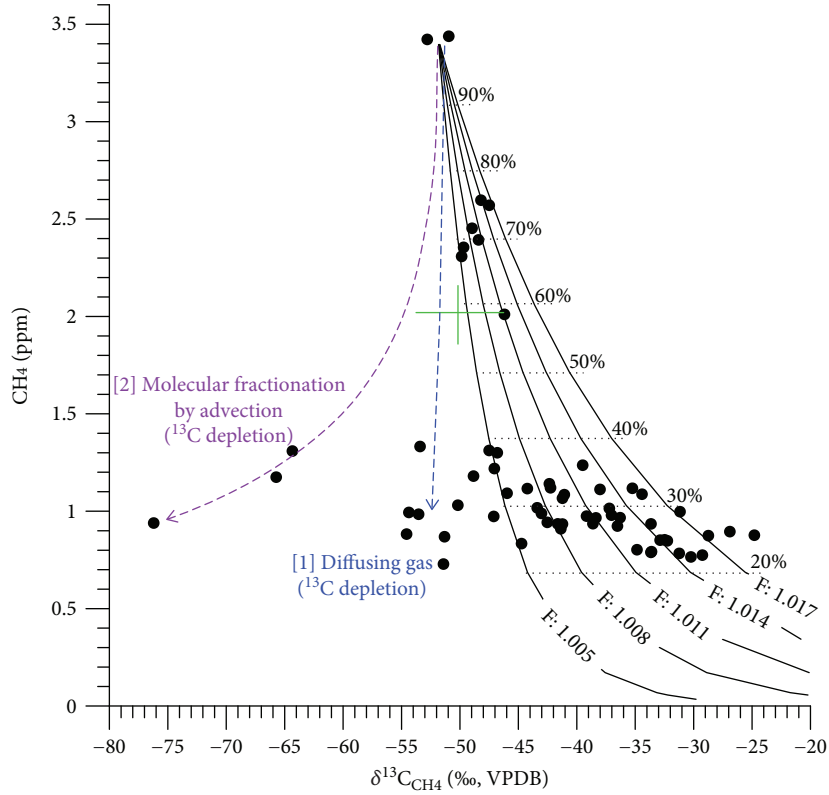

Figure 7: Relationship between CH_4 and δ^{13}C-CH_4 in underground air of Vapour Cave (VC; closed circles). The standard composition of the local background atmosphere is indicated by the green crosshairs (as a reference, the $\delta^{13}C_{CH4}$ value of this crosshairs separates the CH_4 involved in bacterial oxidation from CH_4 coming from other sources). Continuous curves show the locus of compositions formed by methanotrophic consumption of atmospheric methane modelled as a Rayleigh process using several kinetic fractionation factors (F: from 1.005 to 1.017). Horizontal dotted lines with labels show the percentage of deep endogenous methane remaining in cave air after methanotrophic consumption. Curves for isotopic fractionation by diffusion and molecular fractionation by advection are only inferred, but not modelled.

methanogenic aquifers [49]. However, some curves are defined by fractionation factors smaller than those determined in situ in soils [50–52].

Labels of the distillation curves in Figure 7 show the percentage of deep endogenous CH_4 remaining in cave air after its consumption by MOB. In general, cave air samples with subatmospheric CH_4 (<1.3 ppm and $\delta^{13}C_{CH4} > -49‰$, approximately) are consistent with more than 60% removal of the deep endogenous component by bacterial oxidation, i.e., 40% of remaining deep endogenous CH_4. In cave air with the most depleted CH_4 (<0.9 ppm and $\delta^{13}C_{CH4} > -35‰$), the percentage of remaining deep endogenous CH_4 ranges 20–30%. In the case of the outstanding concentrations of deep endogenous CH_4, registered during March of 2016, it is demonstrated that the in situ CH_4 oxidation process was not strong enough to deplete the upwelling flux of this gas below the atmospheric background and, consequently, the percentage of the remaining deep endogenous CH_4 range is above 70%.

The presence of scattered data pairs diverging from the modelled distillation curves (consumption by MOB) in Figure 7 is due to that the closed-system Rayleigh model is an oversimplification of the CH_4 dynamic. It assumes that the upwelling flux of deep endogenous methane is not influenced by other potential inputs and the observed isotopic composition is not affected by other postgenetic processes as isotopic fractionation by diffusion or molecular fractionation by advection. However, oxidation of CH_4 by MOB and the postgenetic modifications seem to occur simultaneously as the upwelling flux of endogenous air travels along the cave profile.

Isotopic fractionation by gas diffusion (curve [1] in Figure 7) is generated during the slow gas movement driven by concentration gradients. The result is a depletion of ^{13}C in diffusing CH_4 (corresponding data pairs diverging from the modelled distillation curves) and ^{13}C enrichment in the residual gas (preferably corresponding to the rest of cave air samples with heavier $\delta^{13}C_{CH4}$). The isotopic fractionation by diffusion generally leads to a slight difference in $\delta^{13}C_{CH4}$, not exceeding 5‰ [53]. This agrees with the $\delta^{13}C_{CH4}$ measurements for the air samples assigned as a result of this process (ranging from 1 to 30 m deep), which does not decrease below −56‰ (Figure 7), i.e., 4.12‰, less than $\delta^{13}C_{CH4}$ for the maximum CH_4 concentration registered at 50 m deep in March 2016 and considered as a clear example of deep endogenous source. In principle, a mixing process between cave air (with depleted CH_4 due to methanotrophic activity) and a potential biogenic source (with

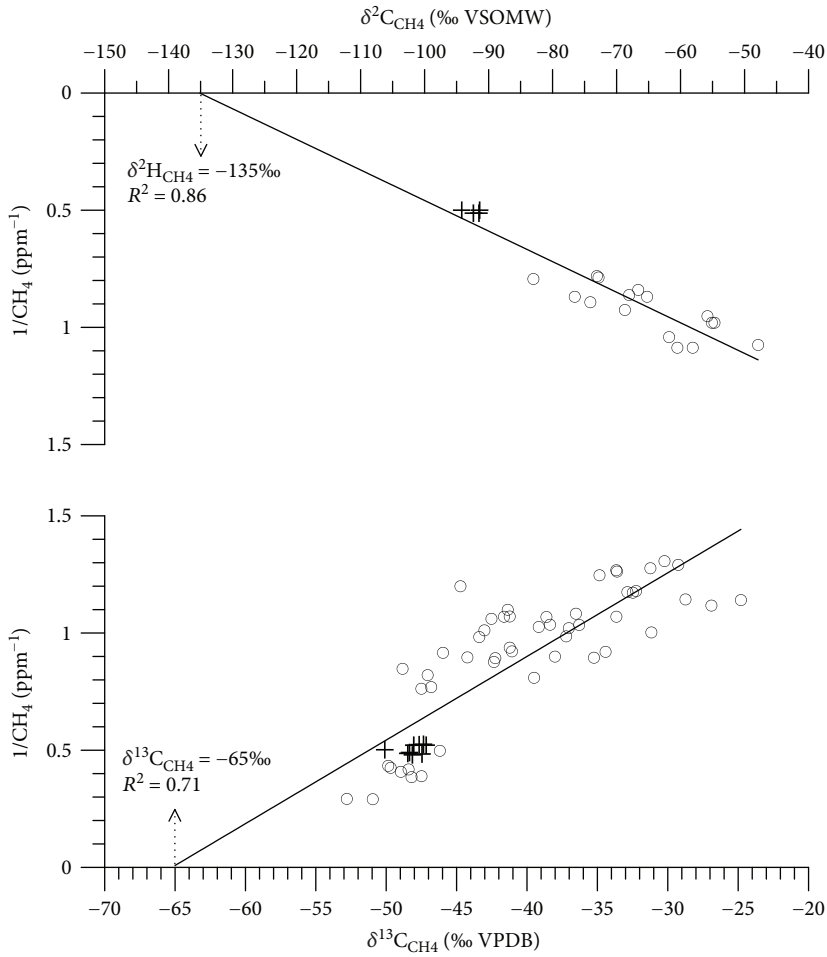

FIGURE 8: Keeling plots of $\delta^{13}C_{CH4}$ and δ^2H_{CH4} from cave air. The open circles represent cave air samples, and crosses represent the outdoor atmosphere. The Keeling plot of $\delta^{13}C_{CH4}$ was made with the entire set of air samples collected throughout the eight field campaigns, whereas the δ^2H_{CH4}-Keeling was plotted with the measurements obtained during the last two field campaigns. The vertical dotted arrows indicate the isotopic compositions ($\delta^{13}C_{CH4}$ and δ^2H_{CH4}) for the source of CH_4 that has been added to the cave air to produce the composition observed at each point.

$\delta^{13}C_{CH4}$ roughly −65‰, according to Figure 8) is discarded because these data points of residual CH_4 with lighter $\delta^{13}C_{CH4}$ do not fit properly with the hypothetical mixing curve between both end-members.

Molecular fractionation by advection is a sort of distillation likely provoked during the vertical transport of the endogenous warm air and upwelling along the cave profile. This process could be responsible for the differential segregation of light CH_4 (data pairs with $\delta^{13}C_{CH4} < 60$‰ that fit curve [2] suggested in Figure 7), and it is exclusively observed for the air samples collected at 2 m depth, i.e., exhaled air from the cave to the open atmosphere.

An alternative mechanism for the isotopic fractionation by gas diffusion may be the low-temperature (<100°C) synthesis of CH_4 related to gas-water-rock reactions, occurring in geothermal areas in continental settings and, even, at shallow depths. Several experimental studies have shown that abiotic CH_4 derived by gas-water-rock reactions can result in $\delta^{13}C_{CH4}$ values as depleted as −57% ([54, 55], and references therein), comparable to the isotopically light values observed in VC and assigned to the isotopic fractionation by gas diffusion (curve [1] at Figure 7). In this sense, a potential inorganic mechanism for CH_4 generation is the hydrogenation of CO_2 in the gas phase (range of temperatures: 25–500°C, according to [54]) and the H_2 necessary for this reaction could be produced by radiolytic decomposition of water vapour (H_20_V) due to the intense radioactive decay. Some of these conditions meet in the subterranean atmosphere of VC: geothermal activity (>35°C), large CO_2 contents (>1%), and high environmental radioactivity (^{222}Rn higher than 50 kBq/m^3). Therefore, further research based on monitoring other ancillary gases as H_2 is essential to providing better insights concerning the potential production of CH_4 related to gas-water-rock reactions that do not directly involve organic matter.

For the next step of data analysis aimed at recognizing the geochemical features of the CH_4 source, the set of [CH_4, $\delta^{13}C_{CH4}$] data pairs identified as a likely result of the aforementioned postgenetic physical processes occurring in the cave profile, i.e., data pairs diverging from the modelled

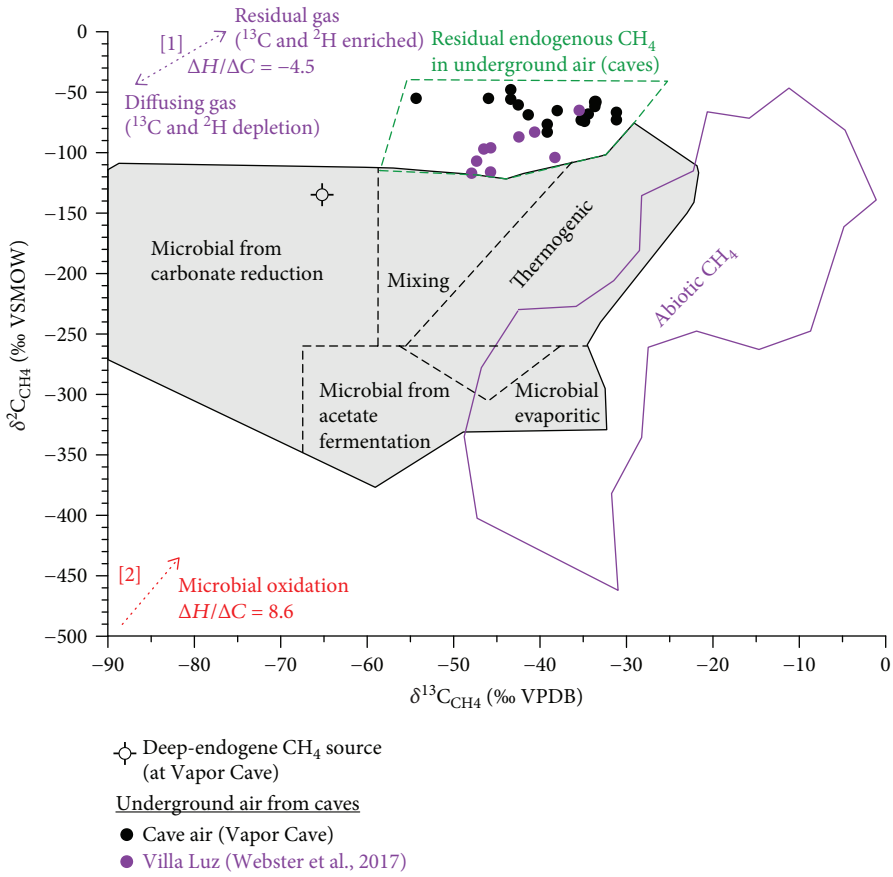

Figure 9: Genetic zonation of CH_4 based on the isotopic composition of carbon ($^{13}C/^{12}C$) and hydrogen ($^{2}H/^{1}H$). Proposed genetic zones of biotic CH_4 (grey zones): thermogenic, microbial from carbonate reduction, microbial from acetate fermentation, and microbial evaporitic, compared to the genetic zone for abiotic CH_4 (modified from [54]). Data pairs of $\delta^{13}C_{CH4}$ and $\delta^{2}H_{CH4}$ are plotted for the local atmosphere, soil air, and underground air of VC in comparison with other published data from hypogenic acid caves [7]. Arrows correspond to two potential postgenetic processes affecting the molecular and isotopic composition of CH_4 after its formation and during its migrations: [A] microbial oxidation and [B] gas diffusion.

distillation curves due to CH_4 consumption by MOB, was not considered (Figure 7).

The relationships between CH_4 concentration and $\delta^{13}C_{CH4}$ and $\delta^{2}H_{CH4}$ values, in both cave air and local atmosphere, fit a two end-member mixing model in Keeling plots (Figure 8). $\delta^{13}C_{CH4}$ in cave air ranged from −53‰ to −25‰, with a subset of points quite similar to the local atmospheric CH_4. $\delta^{2}H_{CH4}$ ranged from −83‰ to −48‰, i.e., with values markedly heavier than the local atmospheric background. The isotopic composition of source CH_4 ($\delta^{13}C_{CH4}$ and $\delta^{2}H_{CH4}$) is estimated with both Keeling plots by extrapolating the linear function that fits the set of data points of cave air and local atmosphere, as far as its intersection with the $\delta^{13}C_{CH4}$ and $\delta^{2}H_{CH4}$ axis, respectively. Accordingly, the isotopic composition estimated for the source that contributes to CH_4 content in cave air is roughly −65‰ ($\delta^{13}C_{CH4}$) and −135‰ ($\delta^{2}H_{CH4}$); i.e., this would correspond to the pure CH_4 that is originally added to the upwelling air that reaches the cave environment and then it is consumed by MOB, independently of other postgenetic alteration processes affecting the concentration and isotopic composition of CH_4 after its formation and emanation from this source (e.g., isotopic fractionation by gas diffusion or molecular fractionation by advection).

The comparative analysis of the stable carbon and hydrogen isotope compositions of methane is an essential diagnostic tool to infer the origin of this gas, even though some additional interpretative parameters are needed for a better understanding, e.g., isotopic composition of associated gases as CO_2. The genetic zonation of CH_4 based on the isotopic composition of carbon ($^{13}C/^{12}C$) and hydrogen ($^{2}H/^{1}H$) was originally introduced by [56] and then developed by [47, 54], among other authors. This analysis approach is aimed at distinguishing the specific signature of biotic methane (thermogenic and microbial) from other potential and diverse abiotic origins of gas (mainly due to volcanic/geothermal activity), besides to infer any sign of postgenetic alteration processes occurring before air is collected into the cave.

Figure 9 shows a diagram of the genetic zonation of CH_4 with a well-defined distribution of carbon and hydrogen isotopes, based on worldwide occurrences of biotic and abiotic methane studied and revised by [54]. The isotopic range of CH_4 observed in VC has been plotted in this diagram,

including local atmosphere, soil air, and underground air. The isotopic composition of the CH_4 source inferred by Keeling plot analyses indicates that methane is primarily formed by bacterial carbonate reduction, likely linked to the Triassic black dolostones below the cave and under an intense water-rock interaction, according to the local hydrogeology settings described above. This kind of biotic methane is typically depleted in ^{13}C relative to thermogenic and other biotic processes and usually range from <−100‰ to about −50‰ [47].

The stable isotopic composition of CH_4 analysed for cave air does not closely match known isotopic compositions typical of microbial (biotic) or abiotic generation and is driven largely by relatively heavier δ^2H_{CH4} values. As a reference, methane in air of VC is even more ^2H-enriched than CH_4 recently described in active acid-hypogenic caves, e.g., Villa Luz [7] (Figure 9). This fact indicates that upwelling CH_4 that reaches VC is the remnant of a larger CH_4 flux at a depth that has been altered during its migration. Therefore, the gas sampled in the cave environment is clearly different from the original gas at the source, whose isotopic features have been previously inferred by Keeling analysis ($\delta^{13}C_{CH4}$: −65‰ and δ^2H_{CH4}: −135‰). The partial consumption of CH_4 and the associated shift in its isotopic compositions contents are likely due to the combination of two postgenetic secondary processes: a prevailing microbial oxidation and, in a less extent, an isotopic fractionation by diffusion. Both processes have been already brought up and inferred by analysing the relationship between CH_4 and $\delta^{13}C_{CH4}$ in underground air, but now they are also corroborated with the comparative analysis of the $\delta^{13}C_{CH4}$ and δ^2H_{CH4} values. Microbial oxidation imparts an increase of about 8.5% in the δ^2H_{CH4} values for every increase of 1% in $\delta^{13}C_{CH4}$ [57, 58]. Gas diffusion, driven by concentration gradients according to Fick's law, may produce ^{13}C and ^2H depletion in the diffusing gas, and a residual gas will be ^{13}C- and ^2H-enriched, according to a $\Delta H/\Delta C$ fractionation slope of 4.5 [54].

The isotopic composition of the deep endogenous source of CH_4 and both fractionation slopes (microbial oxidation and gas diffusion) can be used to infer the alteration pathway of the upwelling CH_4 at VC. Thus, the postgenetic alteration of biotic CH_4 is a consequence of a simultaneous or sequenced effect of both microbial oxidation and gas diffusion. Both processes entail the production of residual methane that is ^{13}C- and ^2H-enriched, and it is primarily present in cave air, whereas the lighter CH_4 (not usually sampled) is either consumed by MOB in a high percentage or is part of diffusing gas exhaled by the cave to the open atmosphere.

7. Conclusions

The gas composition of the subterranean atmosphere at VC is dominantly controlled by the upwelling airflow from the zone of fluid-geodynamic influence of active faulting. Data mining and modelling of variations in the concentrations of the main deep endogenous gases (CO_2, CH_4) and their isotopic signatures ($\delta^{13}C_{CO2}$ and $\delta^{13}C_{CH4}$) have provided considerable insight into the nature of gas exchange between the atmospheric, soil, and underground air gas reservoirs at VC.

Degassing from CO_2-rich groundwater and deep-sourced geothermal CO_2 (mantle-rooted gas) determine the high abundance of this gas at VC (>1%), with a heavier carbon isotopic composition, ranging from −4.5 to −7.5‰. CO_2 in underground air is typically composed of more than 30% of the pure theoretical CO_2 added from a deep endogenous source. The cave acts as a net emitter of CO_2 gas to the local atmosphere, so the exhaled air represents between 1 and 3% of this pure theoretical CO_2 added from a deep endogenous source. The upwelling flow of deep endogenous air also provokes an intense CO_2 diffusion from the cave air into the upper soil layers through fissures and small-size cracks in deep soil-epikarst. Thus, the diffusing CO_2 measured for some soil air samples represent between 5% and 10% of the original deep endogenous CO_2 sourcing the cave environment.

The source of methane in VC has an isotopic signature, which was likely generated by microbial carbonate reduction, likely affecting the Triassic black dolostones below the cave where it is the groundwater level of the local aquifer and, consequently, the water-rock interaction is higher. In this study, we have provided the first evidence demonstrating that caves may occasionally act as net sources of deep endogenous CH_4 to the open atmosphere, with concentrations above the atmospheric background (ranging 2.3–3.4 ppm). This biotic CH_4 is progressively oxidized during its migration through the upper vadose zone. Finally, subatmospheric concentrations of CH_4 were registered in the cave environment. Therefore, hypogenic cave environments may also play a key role in regulating the release of greenhouse gases (e.g., CH_4) to the lower troposphere, through depletion of the concentration of methane with a deep endogenous origin.

Data Availability

The raw data of CO_2 and CH_4 concentrations and their stable isotopic compositions used to support the findings of this study are available from the corresponding author upon request.

Conflicts of Interest

There are no conflicts of interest to declare.

Acknowledgments

This work was supported by the Spanish Ministry of Economy and Competitiveness [projects: GEIs-SUB (CGL2016-78318-C2-1R and CGL2016-78318-C2-2R AEI/FEDER/UE) and CGL2017-83931-C3-2-P]. We thank the GERA group of the Fire-fighters Service of Madrid Autonomous Region for the essential work on installing the system of tubes for air sampling and the Council of "Alhama de Murcia" for their technical assistance during fieldwork.

References

[1] A. Klimchouk, I. Sasowsky, J. Mylroie, S. A. Engel, and A. S. A. Engel, Eds., *Hypogene Cave Morphologies*, Karst Waters Institute Special Publication 18, Karst Waters Institute, Leesburg, VA, USA, 2014.

[2] T. Chavez and P. Reehling, Eds., *Proceedings of Deep Karst 2016: Origins, Resources, and Management of Hypogene Karst, NCKRI Symposium 6*, National Cave and karst research institute, Carlsbad, New Mexico, 2016.

[3] A. Klimchouk, A. N. Palmer, J. WaeleDe, A. S. Auler, and P. Audra, Eds., *Hypogene Karst Regions and Caves on the World. Series: Cave and Karst Systems of the World*, Springer, Switzerland, 2017.

[4] L. D. Hose, A. N. Palmer, M. V. Palmer, D. E. Northup, P. J. Boston, and H. R. DuChene, "Microbiology and geochemistry in a hydrogen-sulphide-rich karst environment," *Chemical Geology*, vol. 169, no. 3-4, pp. 399–423, 2000.

[5] S. Galdenzi, M. Cocchioni, L. Morichetti, V. Amici, and S. Scuri, "Sulfidic ground-water chemistry in the Frasassi caves, Italy," *Journal of Cave and Karst Studies*, vol. 70, pp. 94–107, 2008.

[6] P. Audra, "Hypogene caves in France," in *Hypogene karst regions and caves on the world. Cave and Karst Systems of the World*, A. Klimchouk, A. N. Palmer, J. Waele, A. S. Auler, and P. Audra, Eds., pp. 61–83, Springer, Switzerland, 2017.

[7] K. D. Webster, L. R. Lagarde, P. E. Sauer, A. Schimmelmann, J. T. Lennon, and P. J. Boston, "Isotopic evidence for the migration of thermogenic methane into a sulfidic cave, Cueva de Villa luz, Tabasco, Mexico," *Journal of Cave and Karst Studies*, vol. 79, no. 1, pp. 24–34, 2017.

[8] A. Klimchouk, *Hypogene Speleogenesis: Hydrogeological and Morphogenetic Perspective*, NCKRI special paper series, 1, National Cave and karst research institute, Carlsbad, 2007.

[9] P. Audra and A. N. Palmer, "Research frontiers in speleogenesis. Dominant processes, hydrogeological conditions and resulting cave patterns," *Acta Carsologica*, vol. 44, no. 3, pp. 315–348, 2016.

[10] V. N. Dublyansky, "A giant hydrothermal cavity in the Rhodope Mountains," in *Speleogenesis: Evolution of Karst Aquifers*, Klimchouk, Ford, Palmer, and Dreybrodt, Eds., pp. 317-318, National Speleological Society, Huntsville, 2000.

[11] J. Eensaar, T. Pani, M. Gaškov, H. Sepp, and K. Kirsimäe, "Stable isotope composition of hypogenic speleothem calcite in Kalana (Estonia) as a record of microbial methanotrophy and fluid evolution," *Geological Magazine*, vol. 154, no. 01, pp. 57–67, 2017.

[12] J. Mádlné Szőnyi, A. Erős, T. Havril et al., "Fluidumok, áramlási rendszerek és ásványtani lenyomataik összefüggései a Budai Termálkarszton," *Földtani Közlöny*, vol. 148, no. 1, pp. 75–96, 2018.

[13] M. Gersl, E. Gerslova, D. Hypr, and V. Kolejka, "Sub-crustal CO_2 flux measurement in the Hranice hydrothermal karst," in *21th Goldschmidt Conference "Earth evolution"*, Prague, 2011, European Association of Geochemistry. http://goldschmidt.info/2011/abstracts/G.pdf.

[14] H. Zhu, X. Zhu, and H. Chen, "Seismic characterization of hypogenic karst systems associated with deep hydrothermal fluids in the Middle-Lower Ordovician Yingshan formation of the Shunnan area, Tarim basin, NW China," *Geofluids*, vol. 2017, Article ID 8094125, 13 pages, 2017.

[15] R. Perez-Lopez, J. L. Giner-Robles, M. A. Rodriguez-Pascua et al., "Seismic wave anisotropy caused by the m 5.1 Lorca earthquake (11-5-2011, SE of Spain): testing archaeoseismological techniques with instrumental seismic data," *International Workshop on Active Tectonics, Earthquake Geology, Archaeology and Engineering*, Grützner, F. Steeger, Papanikolaou, Reicherter, Silva, Pérez-López, and Vött, Eds., pp. 190–193, 2011.

[16] R. Perez-Lopez, S. Sanchez-Moral, S. Cuezva et al., "Relationship between the Vapor Cave and the Alhama de Murcia Fault: environmental conditions into de cave versus recent tectonic activity," *Geo-Temas*, vol. 16, no. 1, pp. 363–366, 2016.

[17] T. Rodriguez-Estrella, "Propuesta de aprovechamiento de los recursos geotérmicos de Alhama de Murcia, para que éstos sean renovables," *Nimbus: Revista de climatología, meteorología y paisaje*, vol. 29-30, pp. 577–590, 2012, In Spanish with abstract in English.

[18] M. Martinez-Parra, L. A. Gonzalez, and L. Moreno-Merino, "Balnearios y casas de baño," in *Panorama de las aguas minerales en la región de Murcia, Serie Hidrogeología y Aguas Subterráneas, vol. 5*, J. I. Pinuaga-Espejel and M. Martínez-Parra, Eds., pp. 55–97, Instituto Geológico y Minero de España, Madrid, Spain, 2003, In Spanish, http://aguasmineralesytermales.igme.es/publicaciones/publicaciones-IGME/panorama-aguas-minerales-region-murcia.

[19] J. Baños-Serrano, "Los Baños Termales Minero-Medicinales de Alhama de Murcia," *Memorias de Arqueología*, vol. 5, pp. 354–381, 1995, In Spanish, http://www.patrimur.es/-/memorias-de-arqueologia-5.

[20] I. Abad, F. Nieto, D. R. Peacor, and N. Velilla, "Prograde and retrograde diagenetic and metamorphic evolution in metapelitic rocks of Sierra Espuña (Spain)," *Clay Minerals*, vol. 38, no. 01, pp. 1–23, 2003.

[21] J. C. Ceron, A. Pulido-Bosch, and C. Sanz de Galdeano, "Isotopic identification of CO_2 from a deep origin in thermomineral waters of southeastern Spain," *Chemical Geology*, vol. 149, no. 3-4, pp. 251–258, 1998.

[22] M. Brass and T. Rockmann, "Continuous-flow isotope ratio mass spectrometry method for carbon and hydrogen isotope measurements on atmospheric methane," *Atmospheric Measurement Techniques*, vol. 3, no. 6, pp. 1707–1721, 2010.

[23] A. Fernandez-Cortes, S. Cuezva, M. Alvarez-Gallego et al., "The subsurface atmosphere a methane sink to be considered," *Nature Communications*, vol. 6, no. 7003, 2015.

[24] R. Fisher, D. Lowry, O. Wilkin, S. Sriskantharajah, and E. G. Nisbet, "High-precision, automated stable isotope analysis of atmospheric methane and carbon dioxide using continuous-flow isotope-ratio mass spectrometry," *Rapid Communications in Mass Spectrometry*, vol. 20, no. 2, pp. 200–208, 2006.

[25] R. G. Allen, L. S. Pereira, D. Raes, and M. Smith, "Crop evapotranspiration – guidelines for computing crop water requirements," in *FAO Irrigation and Drainage Paper 56*, FAO, Roma, 1998.

[26] R. Perez-Lopez, M. Patyniak, S. Sanchez-Moral et al.I. Baroň, K. Decker, E. Hintersberger et al., "Relationship between CO_2 content in fault caves and microseismicity," in *Advances in Active Tectonics and Speleotectonics*, p. 28, Natural History Museum Vienna & University of Vienna, Vienna, Austria, 2015.

[27] H.-Y. Wen, T. F. Yang, T. F. Lan et al., "Soil CO_2 flux in hydrothermal areas of the Tatun Volcano Group, Northern Taiwan,"

Journal of Volcanology and Geothermal Research, vol. 321, pp. 114–124, 2016.

[28] M. Zhang, Z. Guo, Y. Sano et al., "Magma-derived CO_2 emissions in the Tengchong volcanic field, SE Tibet: implications for deep carbon cycle at intra-continent subduction zone," *Journal of Asian Earth Sciences*, vol. 127, pp. 76–90, 2016.

[29] R. Botz, G. Winckler, R. Bayer et al., "Origin of trace gases in submarine hydrothermal vents of the Kolbeinsey Ridge, north Iceland," *Earth and Planetary Science Letters*, vol. 171, no. 1, pp. 83–93, 1999.

[30] T. Yokoyama, S. Nakai, and H. Wakita, "Helium and carbon isotopic compositions of hot spring gases in the Tibetan Plateau," *Journal of Volcanology and Geothermal Research*, vol. 88, no. 1-2, pp. 99–107, 1999.

[31] A. Mazot, F. M. Schwandner, B. Christenson et al., "CO_2 discharge from the bottom of volcanic Lake Rotomahana, New Zealand," *Geochemistry Geophysics Geosystems*, vol. 15, no. 3, pp. 577–588, 2014.

[32] D. Cinti, F. Tassi, M. Procesi et al., "Fluid geochemistry and geothermometry in the unexploited geothermal field of the Vicano–Cimino Volcanic District (Central Italy)," *Chemical Geology*, vol. 371, pp. 96–114, 2014.

[33] L. H. Zhang, Z. F. Guo, M. L. Zhang, and Z. H. Cheng, "Study on soil micro-seepage gas flux in the high temperature geothermal area: an example from the Yangbajing geothermal field, South Tibet," *Acta Pretrologica Sinica*, vol. 30, no. 2, pp. 3612–3626, 2014.

[34] D. E. Pataki, J. R. Ehleringer, L. B. Flanagan et al., "The application and interpretation of Keeling plots in terrestrial carbon cycle research," *Global Biogeochemical Cycles*, vol. 17, no. 1, p. 1022, 2003.

[35] R. Amundson, L. Stern, T. Baisden, and Y. Wang, "The isotopic composition of soil and soil-respired CO_2," *Geoderma*, vol. 82, no. 1-3, pp. 83–114, 1998.

[36] E. Garcia-Anton, S. Cuezva, A. Fernandez-Cortes et al., "Abiotic and seasonal control of soil-produced CO_2 efflux in karstic ecosystems located in Oceanic and Mediterranean climates," *Atmospheric Environment*, vol. 164, pp. 31–49, 2017.

[37] M. Camarda, S. de Gregorio, R. Favara, and S. Gurrieri, "Evaluation of carbon isotope fractionation of soil CO_2 under an advective-diffusive regimen: a tool for computing the isotopic composition of unfractionated deep source," *Geochimica et Cosmochimica Acta*, vol. 71, no. 12, pp. 3016–3027, 2007.

[38] C. L. Waring, D. W. T. Griffith, S. Wilson, and S. Hurry, "Cave atmosphere; a guide to calcification and a methane sink," *Geochimica et Cosmochimica Acta*, vol. 73, article A1419, 2009.

[39] C. L. Waring, S. I. Hankin, D. W. T. Griffith et al., "Seasonal total methane depletion in limestone caves," *Scientific Reports*, vol. 7, no. 1, article 8314, 2017.

[40] D. P. Mattey, R. Fisher, T. C. Atkinson et al., "Methane in underground air in Gibraltar karst," *Earth and Planetary Science Letters*, vol. 374, pp. 71–80, 2013.

[41] L. K. McDonough, C. P. Iverach, S. Beckmann et al., "Spatial variability of cave-air carbon dioxide and methane concentrations and isotopic compositions in a semi-arid karst environment," *Environmental Earth Sciences*, vol. 75, no. 8, p. 700, 2016.

[42] J. T. Lennon, D. Nguyễn-Thùy, T. M. Phạm et al., "Microbial contributions to subterranean methane sinks," *Geobiology*, vol. 15, no. 2, pp. 254–258, 2017.

[43] K. D. Webster, A. Mirza, J. M. Deli, P. E. Sauer, and A. Schimmelmann, "Consumption of atmospheric methane in a limestone cave in Indiana, USA," *Chemical Geology*, vol. 443, pp. 1–9, 2016.

[44] D. Nguyễn-Thuỳ, A. Schimmelmann, H. Nguyễn-Văn et al., "Subterranean microbial oxidation of atmospheric methane in cavernous tropical karst," *Chemical Geology*, vol. 466, pp. 229–238, 2017.

[45] E. Hutchens, S. Radajewski, M. G. Dumont, I. McDonald, and J. C. Murrell, "Analysis of methanotrophic bacteria in Movile Cave by stable isotope probing," *Environmental Microbiology*, vol. 6, no. 2, pp. 111–120, 2004.

[46] M. J. Alperin, W. S. Reeburgh, and M. J. Whiticar, "Carbon and hydrogen isotope fractionation resulting from anaerobic methane oxidation," *Global Biogeochemical Cycles*, vol. 2, no. 3, pp. 279–288, 1988.

[47] M. J. Whiticar, "Carbon and hydrogen isotope systematics of bacterial formation and oxidation of methane," *Chemical Geology*, vol. 161, no. 1–3, pp. 291–314, 1999.

[48] N. J. Grant and M. J. Whiticar, "Stable carbon isotopic evidence for methane oxidation in plumes above Hydrate Ridge, Cascadia Oregon Margin," *Global Biogeochemical Cycles*, vol. 16, no. 4, p. 1124, 2002.

[49] K. Urmann, M. H. Schroth, M. Noll, G. Gonzalez-Gil, and J. Zeyer, "Assessment of microbial methane oxidation above a petroleum-contaminated aquifer using a combination of in situ techniques," *Journal of Geophysical Research-Biogeosciences*, vol. 113, no. G2, article G02006, 2008.

[50] W. S. Reeburgh, A. I. Hirsch, F. J. Sansone, B. N. Popp, and T. M. Rust, "Carbon kinetic isotope effect accompanying microbial oxidation of methane in boreal forest soils," *Geochimica et Cosmochimica Acta*, vol. 61, no. 22, pp. 4761–4767, 1997.

[51] J. Chanton and K. Liptay, "Seasonal variation in methane oxidation in a landfill cover soil as determined by an in situ stable isotope technique," *Global Biogeochemical Cycles*, vol. 14, no. 1, pp. 51–60, 2000.

[52] P. J. Maxfield, R. P. Evershed, and E. R. C. Hornibrook, "Physical and biological controls on the in situ kinetic isotope effect associated with oxidation of atmospheric CH4 in mineral soils," *Environmental Science & Technology*, vol. 42, no. 21, pp. 7824–7830, 2008.

[53] G. Etiope, *Natural Gas Seepage: the Earth's Hydrocarbon Degassing*, Springer, 2015.

[54] G. Etiope and B. Sherwood Lollar, "Abiotic methane on earth," *Reviews of Geophysics*, vol. 51, no. 2, pp. 276–299, 2013.

[55] G. Etiope and M. Schoell, "Abiotic gas: atypical, but not rare," *Elements*, vol. 10, no. 4, pp. 291–296, 2014.

[56] M. Schoell, "The hydrogen and carbon isotopic composition of methane from natural gases of various origins," *Geochimica et Cosmochimica Acta*, vol. 44, no. 5, pp. 649–661, 1980.

[57] F. S. Kinnaman, D. L. Valentine, and S. C. Tyler, "Carbon and hydrogen isotope fractionation associated with the aerobic microbial oxidation of methane, ethane, propane and butane," *Geochimica et Cosmochimica Acta*, vol. 71, no. 2, pp. 271–283, 2007.

[58] S. Feisthauer, C. Vogt, J. Modrzynski et al., "Different types of methane monooxygenases produce similar carbon and hydrogen isotope fractionation patterns during methane oxidation," *Geochimica et Cosmochimica Acta*, vol. 75, no. 5, pp. 1173–1184, 2011.

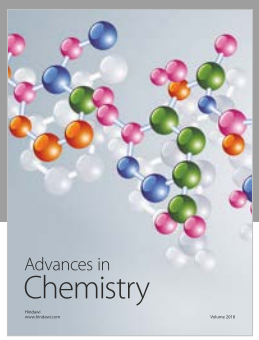

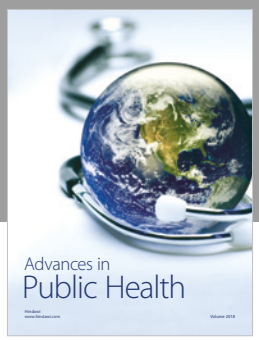

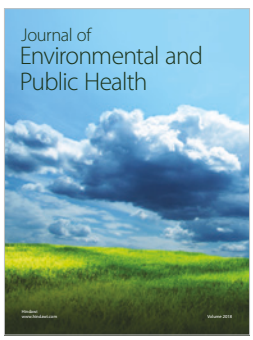

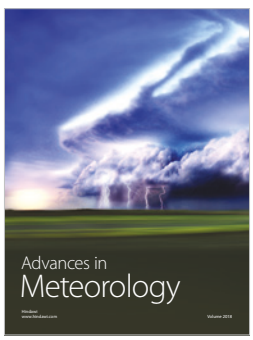

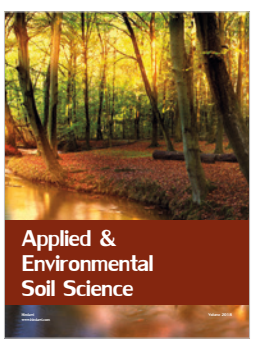

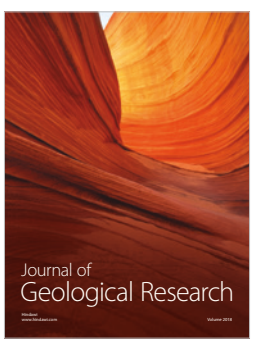

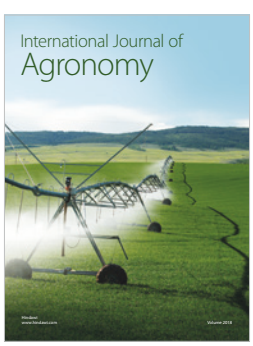

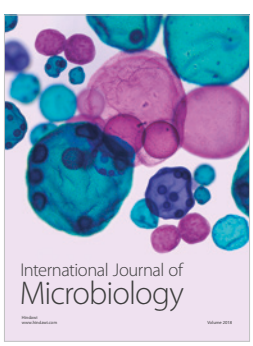

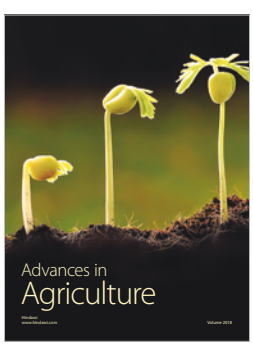

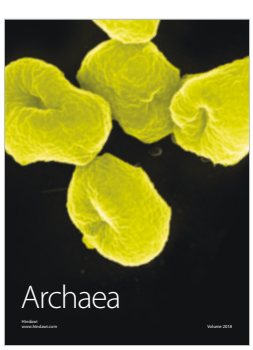

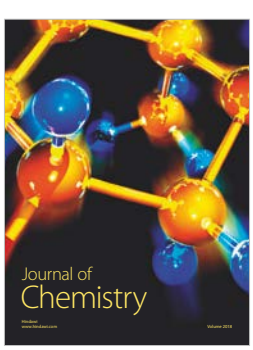


Hindawi

Submit your manuscripts at
www.hindawi.com